Received: 10 December 2024 | Revised: 20 February 2025 | Accepted: 14 March 2025

DOI: 10.1096/fj.202403160R

RESEARCH ARTICLE

The FASEB Journal

Artesunate induces ferroptosis in osteosarcoma through NCOA4-mediated ferritinophagy

Rui Huang[1,2] | **Ruiqing Xu**[3] | **Jiandang Shi**[1] | **Zongqiang Yang**[1,2] | **Jianping Zheng**[1] | **Daihao Wei**[1,2]

[1]Department of Orthopedic Surgery, General Hospital of Ningxia Medical University, Yinchuan, China

[2]The First School of Clinical Medicine, General Hospital of Ningxia Medical University, Yinchuan, China

[3]Department of Orthopedic Surgery, Honghui Hospital, Xi'an Jiaotong University, Xi'an, China

Correspondence
Jiandang Shi, Department of Orthopedic Surgery, General Hospital of Ningxia Medical University, No. 804 Shengli South Street, Xingqing District, Yinchuan, Ningxia, China.
Email: shi_jiandang@nxmu.edu.cn

Funding information
宁夏回族自治区科学技术厅 | Natural Science Foundation of Ningxia Province (宁夏自然科学基金), Grant/Award Number: 2024AAC02069 and 2024AAC03573

Abstract

Osteosarcoma (OS) is a prevalent primary malignant bone tumor that lacks effective therapeutic interventions. Artesunate (ART) has been proved to have remarkable treatment effects on severe malaria and anti-tumor properties. This study aimed to investigate the anti-OS effects and underlying mechanisms of ART. The potential mechanisms of ART-mediated anti-OS activity were analyzed by using RNA sequencing, iron accumulation, lipid peroxidation, western blotting, and small interfering RNA (siRNA) transfection. In vivo, a xenograft mice model was adopted to explore the anticancer effect of ART. The present study revealed that ART significantly suppressed OS cell proliferation. Subsequent results suggested that ART exerted anti-OS activity mainly through the ferroptosis pathway. ART decreased the GSH/GSSG ratio, xCT and GPX4 expression, while increasing MDA and lipid peroxidation, which were reversed by Fer-1, DFO, 3-MA, and NCOA4 silencing. Mechanistically, ART upregulated the expression of TFR and DMT1, and triggered ferritinophagy by upregulating the expression of NCOA4, which increased Fe^{2+} accumulation and triggered ferroptosis. In addition, cytoplasmic iron further activated Mfrn2-mediated transportation of cytoplasmic free iron into the mitochondria, resulting in mitochondrial iron overload, eventually leading to lipid peroxidation and ferroptosis. Furthermore, in an OS xenograft mouse model, administration of ART inhibited tumor growth by ferroptosis. Collectively, our findings indicated that ART has the potential anti-OS capacity through NCOA4-mediated ferritinophagy, which might shed light on the future of OS therapy.

Abbreviations: 3-MA, 3-methyladenine; ART, artesunate; DEGs, differential expression genes; DFO, deferoxamine; DMT1, divalent metal transporter 1; EDTA, ethylenediaminetetraacetic acid; EdU, 5-Ethynyl-2-deoxyuridine; FAC, ferric amine citrate; FDA, food and drug administration; Fer-1, ferrostatin-1; FTH1, ferritin heavy chain-1; Ftmt, mitochondrial ferritin; GO, gene ontology; GPX4, glutathione peroxidase 4; GSH, glutathione; GSSG, L-Glutathione oxidized; KEGG, kyoto encyclopedia of genes and genomes; LSCM, laser scanning confocal microscopy; MDA, malondialdehyde; Mfrn2, mitoferrins 2; MMP, mitochondrial membrane potential; NAC, N-acetylcysteine; NCOA4, nuclear receptor coactivator 4; Nec-1, necrostatin-1; OS, osteosarcoma; PBS, phosphate-buffered saline; PCD, programmed cell death; PCNA, proliferating cell nuclear antigen; PFA, paraformaldehyde; ROS, reactive oxygen species; TFR, transferrin receptor protein.

Rui Huang and Ruiqing Xu contributed equally to this works and share first authorship.

KEYWORDS
artesunate, ferritinophagy, ferroptosis, NCOA4, osteosarcoma

1 | INTRODUCTION

Osteosarcoma (OS) is the most prevalent primary bone malignancy of mesenchymal origin in children and adolescents, with 3.4 cases per million people worldwide.[1,2] Due to the elevated propensity for local recurrence and metastatic dissemination, the utilization of multimodality therapy has seen a surge in application.[3] Currently, the primary approach to treating OS involves a multifaceted therapeutic strategy centered on surgery, coupled with radiotherapy, chemotherapy, targeted therapy, and various other modalities. Although significant progress has been made in the early diagnosis and treatment of OS in recent years, the severe systemic toxicity caused by chemotherapy often makes treatment ineffective, which is one of the important reasons why the recurrence rate and distant metastasis rate of OS patients are still high. Therefore, the development of new effective drugs with low toxicity and effectiveness is an urgent need to improve the efficacy of OS.

Artesunate (ART) was approved by the Food and Drug Administration (FDA) in 2020 as a new treatment for severe malaria.[4] Recent studies have shown that ART exhibits various bioactivities associated with the treatment of cancer, inflammation, and other pharmacological effects.[5,6] Numerous studies have shown that ART could inhibit the proliferation, migration, and invasion of tumor cells by regulating gene expression and signaling pathways, thus playing a therapeutic role in the occurrence and development of various malignant tumors such as liver cancer, lung cancer, and bladder cancer.[7–9] These studies suggested that ART might be an excellent potential candidate for clinical use and anticancer therapy.

Programmed cell death (PCD) plays a significant role in the occurrence, development, and therapy of various malignant tumors.[10] PCD mainly includes pyroptosis, apoptosis, necroptosis, ferroptosis, copper death, and PANoptosis.[11] These forms of cell death differ in both morphology and the mechanisms by which they occur. For example, ferroptosis represents a novel type of PCD distinguished by its dependence on iron and the accumulation of intracellular oxidants.[12] Compared with normal cells, a high concentration of an unstable iron pool is an important substance and metabolic basis for abnormal proliferation, drug resistance, and the maintenance of tumor stem cells.[13] Ferroptosis may thus be proposed as an alternative intervention for cancer therapy. Currently, there are several FDA-approved drugs that target ferroptosis, such as erastin and deferoxamine mesylate (DFO). However, their unsatisfactory chemical properties, severe adverse reactions, and poor tumor targeting limit their clinical application. It is surprising that several natural chemicals could suppress tumor growth by the ferroptosis pathway, such as red ginseng polysaccharide,[14] agrimonolide,[15] tiliroside[16] and ginsenoside Rh3.[17] Similarly, our previous study showed that shikonin suppresses the proliferation of OS cells by inducing ferroptosis through promoting Nrf2 ubiquitination and inhibiting the xCT/GPX4 regulatory axis.[18] To date, it has been reported that ART exhibits antitumor effects by inducing ferroptosis in multiple myeloma.[19] Nevertheless, the ability of ART to inhibit the proliferation of OS cells, the specific cell death pathways involved, and the underlying mechanisms remain unknown.

In the present study, ART is reported for the first time to suppress OS cell growth in vitro and in vivo, primarily through the ferroptosis pathway. The findings could provide new insights for further improving the prognosis of patients with OS and provide a theoretical basis and solid foundation for the clinical application of ART.

2 | MATERIALS AND METHODS

2.1 | Cell lines and cell culture

Osteoblast cell line hFOB1.19 was obtained from the American Type Culture Collection (ATCC). OS cell lines MG63 and 143B were acquired from Procell (Wuhan, China). All cells were cultured in dulbecco's modified eagle medium (DMEM) (Vivacell Bioscience, Shanghai, China). In addition to DMEM, complete culture medium comprised 1% penicillin (Vivacell, Shanghai, China) and 10% fetal bovine serum (FBS) (Thermo Fisher, Shanghai, China). The culture conditions were maintained at 5% CO_2 and a temperature of 37°C.

2.2 | Reagents and antibodies

ART, 3-methyladenine (3-MA), ferrostatin-1 (Fer-1), DFO, Z-VAD, necrostatin-1 (Nec-1) and N-acetylcysteine (NAC) purchased from MedChemExpress (MCE, State of New Jersey, USA), ferric amine citrate (FAC) was purchased from Yuanye Biotec (Shanghai, China), and the drug was

dissolved in DMSO and stored at −20°C for usage. The primary antibodies used in the experiments included β-actin (Proteintech, Wuhan, China), GAPDH (Proteintech, Wuhan, China), proliferating cell nuclear antigen (PCNA) (Proteintech, Wuhan, China), recombinant glutathione peroxidase 4 (GPX4) (Proteintech, Wuhan, China), xCT (Proteintech, Wuhan, China), nuclear receptor coactivator 4 (NCOA4) (Affinity, Jiangsu, China), microtubule-associated proteins 1A/1B light chain 3I/II (LC3I/II) and P62 (Cell Signaling Technology, USA), transferrin receptor (TFR) (Proteintech, Wuhan, China), divalent metal transporter 1 (DMT1) (Absin, Shanghai, China), ferritin heavy chain 1 (FTH1) (Cell Signaling Technology, USA), Mitoferrins 2 (Mfrn2) and mitochondrial ferritin (Ftmt) (Absin, Shanghai, China).

2.3 | Cell transfection

The siRNAs targeting NCOA4 and Mfrn2 (designated as siNCOA4 and siMfrn2, respectively) and non-targeting control siRNAs (siNC) were synthesized by Sangon Biotech (Shanghai, China). Following the manufacturer's instructions, RNA transfection was carried out using Lipofectamine 3000 reagent (Thermo Fisher Scientific) for a duration of 48 h.

2.4 | Cell viability assay

MG63, 143B, and hFOB 1.19 cells were treated with or without ART for 24, 48, or 72 h, and the concentrations of ART were (0, 5, 10, 20, 30, 40, 60, 80, and 100 μM). According to the pretest results, the optimal drug concentration and drug action time of each group were determined. According to the experimental design, cells in each group were treated with the corresponding drug. Following this treatment, the drug-containing medium was removed, and a CCK-8 solution was diluted in accordance with the provided instructions. The cells were then incubated for a duration of 2 h. Then, the absorbance was measured at 450 nm by an enzyme-labeled apparatus. Data collection and statistics were performed using GraphPad Prism 8.0 software (San Diego, CA, USA).

2.5 | Giemsa staining

Giemsa staining was performed to observe the impact of ART on the change in cell morphology. MG63 and 143B were plated in 12 well plates. ART was added to MG63 and 143B cells at varying concentrations (0, 20, 40, 80 μM) for a duration of 24 h after the cells were completely adhered to the wall. After being fixed for 20 min in 4% paraformaldehyde (PFA) (Solarbio, Beijing, China), the cells were stained for 20 min with 1% Giemsa staining solution (Solarbio, Beijing, China), and they were gently rinsed 3 times with phosphate-buffered saline (PBS). Cell morphology was evaluated using an optical microscope (Olympus Corporation, Tokyo, Japan).

2.6 | Colony formation assay

MG63 and 143B cells, during their logarithmic growth phase, were inoculated into 6-well plates at a density of 500 cells per well in the form of a single-cell suspension. Following a 48 h incubation period, these cells were treated with various concentrations of ART or a vehicle control, with each group consisting of three wells. The cells were subsequently maintained for two weeks, with the growth medium being refreshed every three days. After this treatment period, the cells were fixed using 4% PFA and stained with 0.1% crystal violet (Solarbio, China) for a duration of 10 min. The staining results were analyzed using Image J software.

2.7 | Cell cycle analysis

MG63 and 143B were thoroughly mixed with the medium and inoculated on 6-well plates. Once the cells reached 80% confluence, the complete medium was removed, the wells were rinsed with PBS, and the cells were incubated with the corresponding drug-containing medium for 24 h. After this incubation, the medicated medium was discarded. The cells were then digested, centrifuged at low speed, transferred to 1.5 mL sterile culture tubes, and treated with anhydrous ethanol overnight. Subsequently, PI and RNase A were added and incubated according to the kit instructions. Finally, the cell cycle of each group was assessed using flow cytometry with the Accuri C6 Plus instrument and analyzed quantitatively. For details, please refer to our previous study.[18]

2.8 | RNA sequencing

MG63 cells were treated with 40 μM of ART for a duration of 24 h. Following this treatment, RNA was extracted from the cells using TRIzol reagent, which was sourced from ThermoFisher Scientific (USA). The extracted RNA samples were then stored on dry ice. Subsequently, the process of library construction and RNA sequencing was carried out by Biomarker Technologies (Biomarker, Beijing, China).

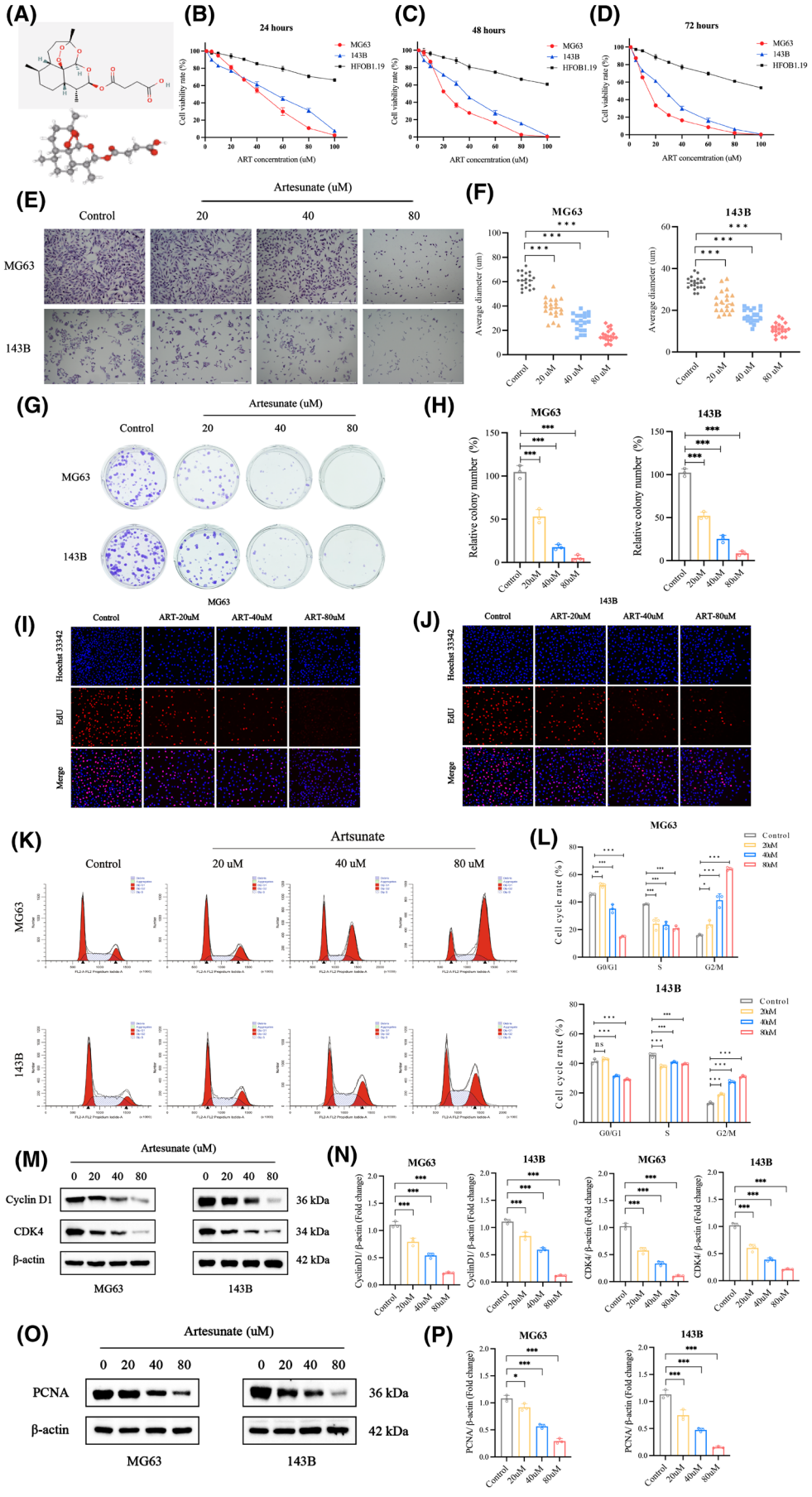
(A)
(B)
24 hours
MG63
143B
HFOB1.19
Cell viability rate (%)
ART concentration (uM)
(C)
48 hours
(D)
72 hours
(E)
Artesunate (uM)
Control
20
40
80
MG63
143B
(F)
MG63
143B
Average diameter (um)
Control
20 uM
40 uM
80 uM
(G)
Artesunate (uM)
Control
20
40
80
MG63
143B
(H)
MG63
143B
Relative colony number (%)
Control
20uM
40uM
80uM
(I)
MG63
Control
ART-20uM
ART-40uM
ART-80uM
Hoechst 33342
EdU
Merge
(J)
143B
(K)
Artsunate
Control
20 uM
40 uM
80 uM
MG63
143B
(L)
MG63
143B
Control
20uM
40uM
80uM
Cell cycle rate (%)
G0/G1
S
G2/M
(M)
Artesunate (uM)
0 20 40 80
Cyclin D1
CDK4
β-actin
36 kDa
34 kDa
42 kDa
MG63
143B
(N)
MG63
143B
CyclinD1/ β-actin (Fold change)
CDK4/ β-actin (Fold change)
Control
20uM
40uM
80uM
(O)
Artesunate (uM)
0 20 40 80
PCNA
β-actin
36 kDa
42 kDa
MG63
143B
(P)
MG63
143B
PCNA/ β-actin (Fold change)
Control
20uM
40uM
80uM

FIGURE 1 ART inhibited the proliferation of OS cells. (A) The molecular and 3D structure of ART. (B–D) The effect of ART on the viability of MG63,143B and HFOB1.19 cells was measured by CCK-8 assay after being treated for 24, 48, and 72 h. (E, F) Giemsa staining was used to observe the effect of ART on the cell morphology of MG63 and 143B. (G, H) Colony formation and (I, J) EdU staining were used to observe the impact of ART on the cell proliferation of MG63 and 143B. (K, L) The cell cycle was evaluated in MG63 and 143B cells using flow cytometry analysis with PI staining. (M, N) Western blot was used to detect the expression of the cell cycle protein Cyclin D1 and CDK4. (O, P) Western blot was used to detect the expression of the proliferation protein PCNA. Data represent mean ± SD. Significance in (B–D), (F), (H), (L), (N) and (P) was calculated using one-way ANOVA with Dunnett's multiple comparisons test. $n = 3$; $^{*}p < .05$; $^{**}p < .01$; $^{***}p < .001$; ns, no significant.

2.9 | Transmission electron microscopy

According to the experimental protocol, MG63 and 143B cells were inoculated into culture dishes. MG63 and 143B cells were treated with or without 40 μM ART for 24 h. Following their digestion with pancreatic enzymes free of ethylenediaminetetraacetic acid (EDTA), the cells were centrifuged. Subsequent steps included the immobilization and dehydration of the cell masses using anhydrous ethanol. Finally, after processing the samples, the cell structures were observed by a transmission electron microscope (Olympus Corporation, Tokyo, Japan).

2.10 | 5-Ethynyl-2-deoxyuridine (EdU) assay

MG63 and 143B cells were plated in a 24-well plate at a density of 5×10^4 cells per well. Following a 24 h drug treatment, EdU working solution was added to the cells, and they were incubated at 37°C for 2 h. The cells were then fixed with methanol for 30 min and permeabilized with Triton-X for 40 min to allow for the penetration of staining reagents. Next, a click reaction solution was added and incubated for 40 min to label the EdU-incorporated DNA. Subsequently, the cells were stained with Hoechst-33342 solution to visualize the nuclei. Finally, all samples were observed and imaged under a confocal microscope provided by Nikon (Japan).

2.11 | Flow cytometric analysis of detecting reactive oxygen species (ROS), lipid peroxidation, mitochondrial membrane potential (MMP), Fe^{2+} content and FITC-Annexin V/PI staining assay

Flow cytometry was applied to detect ROS, lipid peroxidation, apoptosis, and Fe^{2+}. Briefly, for the detection of ROS, cells were stained with DCFH-DA (10 μM) (Invitrogen, Carlsbad, CA, United States) for 30 min at 37°C in the dark. For the detection of intracellular lipid peroxidation, C11-BODIPY (Thermo Fisher Scientific, Waltham, USA) was used to detect the level of lipid peroxidation. JC-1 (KeyGEN BioTECH, Jiangsu, China) was used to detect the level of MMP. FerroOrange is a product offered by DOJINDO (Shanghai, China) for quantifying the concentrations of different groups of Fe^{2+}. The method uses FerroOrange (1 μM) as a colorimetric agent, changes its color according to the presence of Fe^{2+}, and determines its concentration by flow cytometry. The FITC-Annexin V/PI staining assay was used to detect the effect of ART on OS cell apoptosis. Collected data were analyzed using FlowJo 10.7.1 software.

2.12 | Measurement of malondialdehyde (MDA) levels and GSH/GSSG ratio

Intracellular concentrations of MDA and the GSH/GSSG ratio were measured using specific assay kits (Jiancheng, Nanjing, China). The MDA assay kit and the GSH/GSSG ratio assay kit were employed, and all measurements were conducted in accordance with the detailed instructions provided by the manufacturer.

2.13 | Immunofluorescence analysis

Intracellular Fe^{2+} and mitochondrial Fe^{2+} levels were detected using FerroOrange (Dojindo, Shanghai, China) and Mito-FerroGreen (Dojindo, Shanghai, China) respectively. According to the protocol, the cells were seeded in confocal dishes, and after corresponding treatment with drugs for 24 h, the cells were incubated with FerroOrange (0.5 μM) or Mito-FerroGreen for 30 min. For the detection of mitochondrial ROS, the cells were incubated with 5 μM Mito-SOX (Dojindo, Shanghai, China) for 30 min. Following the incubation period, the cells were observed under a confocal microscope (Nikon, Japan) to visualize and quantify the Mito-SOX fluorescence, which is indicative of mitochondrial ROS levels.

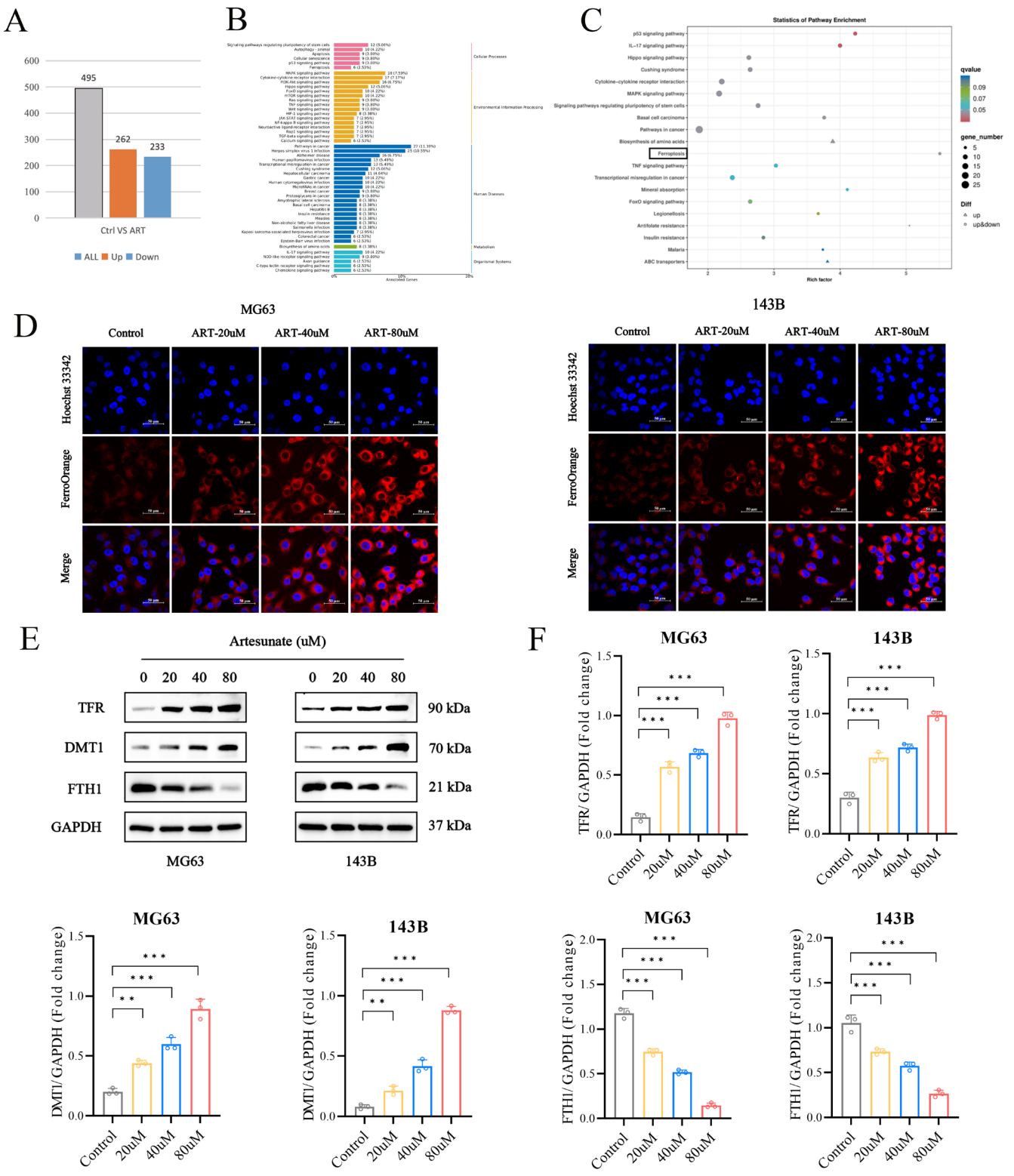

FIGURE 2 ART inhibited the proliferation of OS cells through the ferroptosis pathway. (A) DEGs following treatment with ART (40 μM) for 24 h compared to controls (DMSO for 24 h) in MG63 cells, assessed via RNA sequencing assay. (B) The GO enrichment analysis of DEGs. (C) Top 20 KEGG pathway enrichment results of DEGs. (D) Intracellular Fe^{2+} was observed by using laser scanning confocal microscopy (LSCM) after the intervention of ART after 24 h in MG63 and 143B cells (scale bar: 50 μm). (E, F) Western blot was used to detect the expression of ferroptosis proteins TFR, DMT1, and FTH1. Data represent mean ± SD; significance in (F) was calculated using one-way ANOVA with Dunnett's multiple comparisons test. $n = 3$; $^{**}p < .01$; $^{***}p < .001$.

2.14 | Western blot assay

MG63 and 143B cells were inoculated in cell culture dishes. Once the cells were fully adhered to the surface, they were treated with the corresponding drugs for 24 h, in accordance with the experimental design. Subsequently, the samples were washed with pre-cooled PBS, and the cells were digested and collected using pancreatic enzymes. Then, following the instructions in the manual, protein quantification was performed using the BCA protein quantification kit method. The SDS-PAGE gel was prepared according to the guidelines provided by the reagent manufacturer. After the electrophoresis of the sample was completed, the gel containing the sample was placed on a polyvinylidene fluoride membrane for the transfer step. Samples were incubated with 5% buttermilk for a duration of 2 h. The sample should be gently agitated overnight on a shaker at a temperature of 4°C. The samples that had been incubated with the corresponding secondary antibodies were allowed to incubate for 2 h, after which they were again washed with TBST. Subsequently, exposure and image acquisition were performed. The results were processed using Image Lab and Image J software. For details, please refer to our previous study.[18]

2.15 | OS intra-tibia tumor-bearing model

This animal experiment was conducted in accordance with the guidelines outlined in the National Institutes of Health (NIH) publication "Guide for the Care and Use of Laboratory Animals" (NIH Publications No. 8023, revised 1978). It received approval from the Animal Ethics Committee of Wuhan Sevier Biotechnology Co. (2024030 on March 7, 2024). A total of 20 BALB/c nude mice, aged 4–5 weeks, were purchased for the study. Each mouse received an injection of 1×10^6 143B cells in a volume of 100 μL into the tibial bone marrow cavity. Once the tumors became palpable or measurable, the animals were randomly assigned to four groups, with five mice in each group: the control group (10% DMSO + 40% PEG300 + 5% Tween-80 + 45% Saline), the Fer-1 group (0.8 mg/kg/day), the ART group (200 mg/kg/day) and the ART+Fer-1 group. Each group of mice received daily intraperitoneal injections of the drug for 2 weeks. The weight of the mice and the volume of the tumors were measured every three days. Tumor volume (mm^3) was calculated using the formula: (length × width^2)/2, where "length" represents the longest axis of the tumor and "width" is the measurement perpendicular to the length. Once the experiment was completed, the mice were euthanized, and all tumors were collected for further analysis.

2.16 | Histological examination and immunohistochemistry

The collected tumor samples were fixed in 5% formaldehyde overnight to preserve their structure and morphology. Following fixation, the tumor tissues were subjected to a gradient alcohol dewatering method to remove excess water and facilitate embedding in paraffin wax. The paraffin-embedded tissues were then sectioned to produce thin slices for further analysis. After sodium citrate buffer repair, peroxides were added to seal. Next, specific primary and secondary antibodies were added to target and bind to the antigens of interest within the tissue. DAB working solution was added, and hematoxylin staining was performed. Finally, images of the stained sections were captured under a microscope for further analysis.

2.17 | Statistical analysis

The data obtained from these experiments were presented as the mean ± standard deviation (SD). To determine whether there were significant differences among the groups, a one-way or two-way analysis of variance (ANOVA) was performed. This statistical test allows for the comparison of multiple groups and assesses whether there are any statistically significant differences in the mean values among the groups. If a significant difference was determined by the ANOVA, multiple-comparison tests were applied to identify which specific pairs of groups were significantly different. $^*p < .05$, $^{**}p < .01$, and $^{***}p < .001$.

3 | RESULTS

3.1 | ART inhibited the proliferation of OS cells

The molecular structure and 3D structure of ART were obtained from the PubChem database (https://pubchem.ncbi.nlm.nih.gov) (Figure 1A). To explore the effect of ART on the cell viability of OS cells and the osteoblast cell line HFOB1.19, we applied different concentrations of ART (0, 5, 10, 20, 30, 40, 60, 80 and 100 μM) to intervene. The CCK-8 assay suggested that the cell viability of MG63 and 143B cells decreased in a dose-dependent and time-dependent manner after ART treatment. The IC_{50} values of MG63, 143B, and HFOB1.19 cells treated with ART for 24 h were 40.12, 45.9 and 167.4 μM (Figure 1B–D). Therefore, 20, 40 and 80 μM concentrations of ART were selected for the following experiments. Giemsa staining indicated that cell morphology crumpled and the nucleus had deep staining, decreased OS cell status, and viability

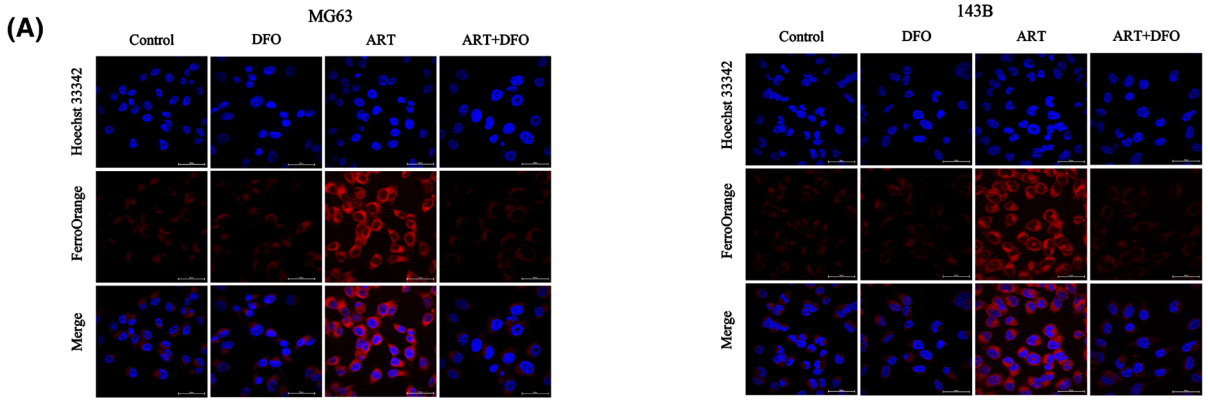
(A)
MG63
143B
Control
DFO
ART
ART+DFO
Hoechst 33342
FerroOrange
Merge

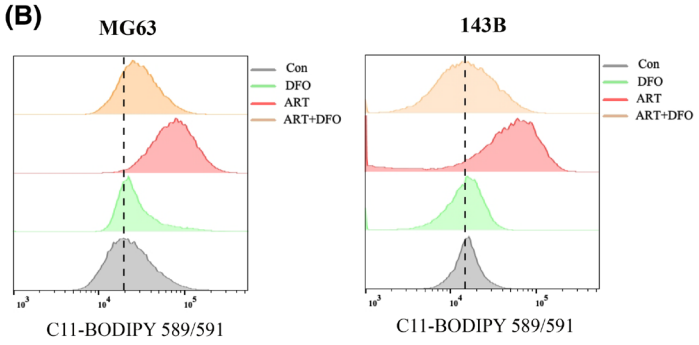
(B)
MG63
143B
Con
DFO
ART
ART+DFO
C11-BODIPY 589/591

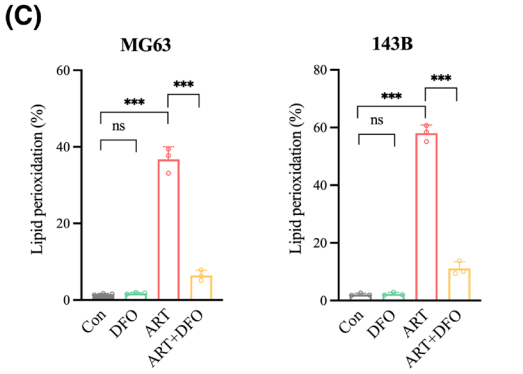
(C)
MG63
143B
Lipid perioxidation (%)
ns
***
Con
DFO
ART
ART+DFO

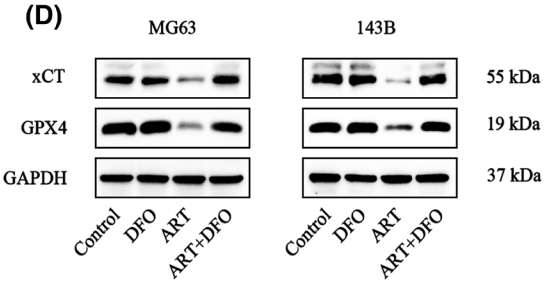
(D)
MG63
143B
xCT
GPX4
GAPDH
55 kDa
19 kDa
37 kDa
Control
DFO
ART
ART+DFO

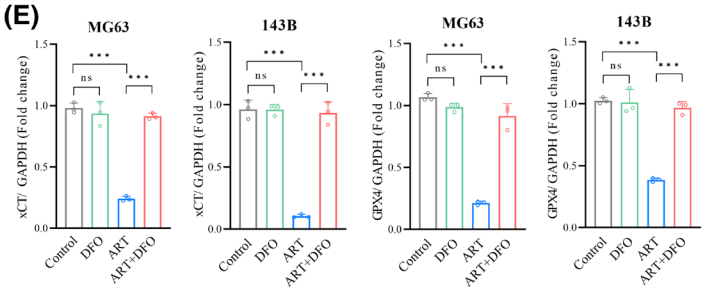
(E)
MG63
143B
xCT/ GAPDH (Fold change)
GPX4/ GAPDH (Fold change)
ns
***
Control
DFO
ART
ART+DFO

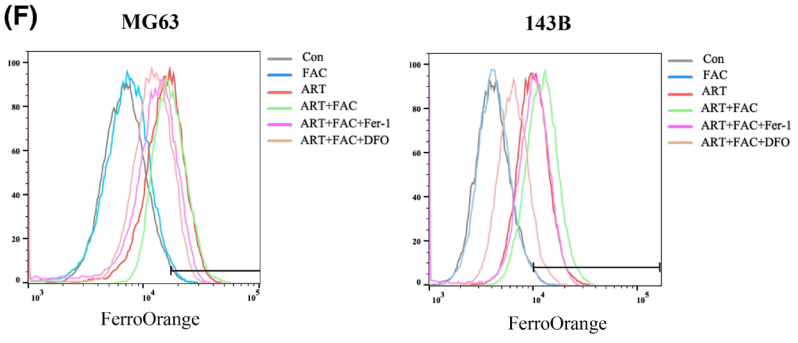
(F)
MG63
143B
Con
FAC
ART
ART+FAC
ART+FAC+Fer-1
ART+FAC+DFO
FerroOrange

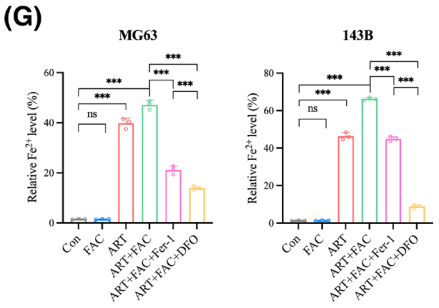
(G)
MG63
143B
Relative Fe2+ level (%)
ns
***
Con
FAC
ART
ART+FAC
ART+FAC+Fer-1
ART+FAC+DFO

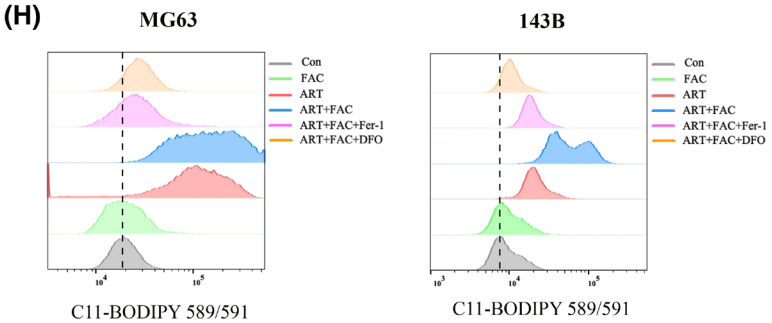
(H)
MG63
143B
Con
FAC
ART
ART+FAC
ART+FAC+Fer-1
ART+FAC+DFO
C11-BODIPY 589/591

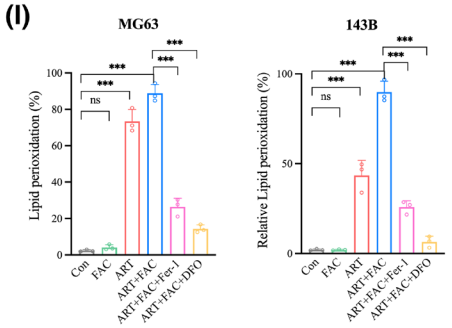
(I)
MG63
143B
Lipid perioxidation (%)
Relative Lipid perioxidation (%)
ns
***
Con
FAC
ART
ART+FAC
ART+FAC+Fer-1
ART+FAC+DFO

FIGURE 3 Decreased intracellular iron levels protected OS cells against ART-induced ferroptosis. (A) Intracellular Fe^{2+} was observed by using LSCM after the intervention of ART with or without DFO after 24 h in MG63 and 143B cells (scale bar: 50 μm). (B, C) Lipid peroxidation was evaluated in MG63 and 143B cells after the intervention of ART with or without DFO after 24 h by using flow cytometry analysis with C11-BODIPY 589/591 staining, followed by quantitative analysis. (D, E) Western blot was used to detect the expression of protein xCT and GPX4, and quantification was analyzed. (F, G) Intracellular Fe^{2+} and (H, I) Lipid peroxidation were observed by flow cytometry after the intervention of the drug after 24 h in MG63 and 143B cells. Data represent mean ± SD; significance in (C), (E) (G) and (I) was calculated using the one-way ANOVA with Dunnett's multiple comparisons test. $n = 3$; $^{***}p < .001$.

after ART intervention for 24 h (Figure 1E,F). The results of the colony formation assay were consistent with those of the CCK-8 assay (Figure 1G,H) and EdU proliferation assays (Figure 1I,J). The flow cytometry assay showed that ART could induce cell cycle arrest at the G1→S phase, decrease the percentage of cells in the G1 phase, and increase the percentage of cells in the S and G2/M phases in MG63 and 143B (Figure 1K,L). Further research found that ART downregulated the expression of Cyclin D1 and CDK4 (Figure 1M,N). PCNA is a cofactor of DNA polymerase and plays important roles in DNA replication and cell proliferation.[20] In the present study, we found that ART significantly downregulated the expression of PCNA in MG63 and 143B in a dose-dependent manner (Figure 1O,P). In addition, we examined whether ART could induce apoptosis of OS cells, and the results showed that ART induced apoptosis of OS cells in a dose-dependent manner, but the proportion of apoptotic cells was still very low under the action of ART (80 μM), which indicated that ART may inhibit the proliferation of OS cells mainly through pathways other than apoptosis (Figure S1A,B).

3.2 | ART inhibited OS cell proliferation mainly through the ferroptosis pathway

In order to explore the main ways that ART inhibits the proliferation of OS cells, transcriptome sequencing and bioinformatics analysis were performed to identify the differentially expressed genes (DEGs) in the control and ART treated cells with MG63. 262 upregulated genes and 233 downregulated genes were detected in ART-treated cells compared with cells of the control group (Figure 2A). The gene ontology (GO) enrichment analysis of DEGs was illustrated (Figure 2B). The results of the Kyoto Encyclopedia of Genes and Genomes (KEGG) pathway enrichment analysis were visualized on a bubble map, with the top 20 most significantly changed pathways displayed (Figure 2C). Notably, ferroptosis emerged as one of the most altered pathways. Given its close association with cancer therapy, it is plausible that ferroptosis could serve as the primary mechanism underlying ART-induced OS cell death. To further confirm which form of cell death is induced by ART, this study combined ART with different cell death inhibitors for CCK-8 rescue experiments, including Z-VAD (10 μM), Nec-1 (10 μM), 3-MA (1 mM), DFO (50 μM), NAC (5 mM) and Fer-1(10 μM). Further studies showed that ferroptosis-related inhibitors Fer-1, DFO, and the autophagy inhibitor 3-MA significantly reversed the inhibitory effect of ART on the proliferation of OS cells (Figure S1C). Moreover, the combination of Fer-1 with 3-MA had a synergistic effect on reversing the inhibition of OS cell proliferation by ART (Figure S1D). Together, these results suggested that ferroptosis and autophagy are the main pathways by which ART inhibits the proliferation of OS cells.

The disturbance of intracellular iron metabolism, especially the increase of ferrous ion content, is the initial factor of ferroptosis. The Fenton reaction, which involves the interaction of Fe^{2+} with endogenous hydrogen peroxide (H_2O_2), generates ROS. These ROS can subsequently promote lipid peroxidation, a critical process in the induction of ferroptosis.[21] We detected a significant increase in intracellular Fe^{2+} levels after ART treatment in a concentration-dependent manner (Figure 2D). TFR, a membrane protein expressed as a homodimer on the cell surface, binds to transferrin and mediates the internalization of iron into the cell. This process is crucial for cellular iron uptake and plays a significant role in regulating oxidative stress levels. Once inside the cell, the intracellular metal reductase STEAP3 reduces Fe^{3+} to Fe^{2+}, which is then released into the dynamic iron pool of the cytoplasm via DMT1.[22] Excess Fe^{2+} are mainly stored in FTH1 to inhibit iron overload and ferroptosis in cells.[23] Western blot results showed that ART treatment for 24 h could upregulate the expression of TFR, DMT1 proteins and downregulate the expression of FTH1 protein in OS cells (Figure 2E,F).

3.3 | Decreased intracellular iron levels protect OS cells against ART-induced ferroptosis

Fe^{2+} plays an important role in ferroptosis; we co-treated OS cells with DFO and ART (40 μM) to decrease intracellular iron concentration. Intracellular Fe^{2+} levels increased significantly after ART treatment and were effectively rescued by DFO (Figure 3A). Similarly, the DFO-treated group reversed ART-induced lipid peroxidation accumulation (Figure 3B,C). In line with this, ART

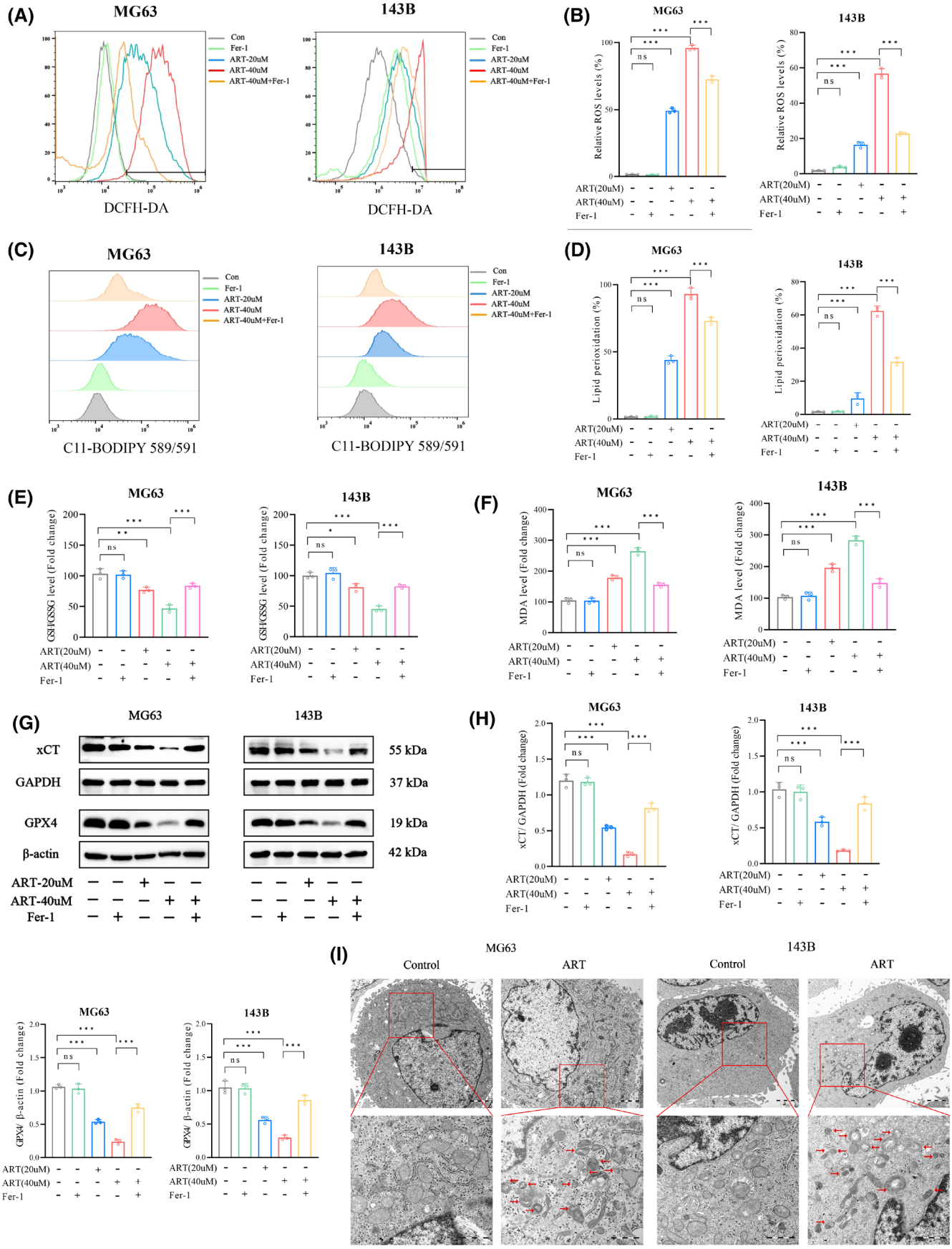
(A)
MG63
143B
Con
Fer-1
ART-20uM
ART-40uM
ART-40uM+Fer-1
DCFH-DA
(B)
Relative ROS levels (%)
(C)
C11-BODIPY 589/591
(D)
Lipid perioxidation (%)
(E)
GSH/GSSG level (Fold change)
(F)
MDA level (Fold change)
(G)
xCT
GAPDH
GPX4
β-actin
55 kDa
37 kDa
19 kDa
42 kDa
(H)
xCT/ GAPDH (Fold change)
GPX4/ β-actin (Fold change)
(I)
Control
ART
ART(20uM)
ART(40uM)
Fer-1

FIGURE 4 Fer-1 reversed ART-induced ferroptosis in OS cells. (A, B) The ROS and (C, D) lipid peroxidation were evaluated in MG63 and 143B cells by using flow cytometry analysis with DCFH-DA or C11-BODIPY 589/591 staining, followed by quantitative analysis. (E) Measurement of intracellular GSH/GSSG levels in MG63 and 143B cells. (F) Measurement of intracellular MDA levels in MG63 and 143B cells. (G, H) Western blot was used to detect the expression of protein xCT and GPX4, and quantification was analyzed. (I) The mitochondrial morphology of MG63 and 143B cells treated with or without ART after 24 h was observed by transmission electron microscopy (Scale bar: 1 μm). Data represent mean ± SD, and significance in (B), (D), (E), (F) and (H) were calculated using the one-way ANOVA with Dunnett's multiple comparisons test. $n = 3$; *$p < .05$; **$p < .01$; ***$p < .001$.

downregulated the expression of xCT and GPX4 proteins in OS cells, which could be significantly reversed by DFO (Figure 3D,E). In summary, these results suggested that ART induced ferroptosis by causing iron overload in OS cells.

To further determine the role of iron in the ART-induced ferroptosis, we treated OS cells with non-toxic concentrations of FAC (100 μM) to increase intracellular iron concentration combined with ART. Our results indicated that FAC exacerbated ART-induced suppression of OS cell activity and could be partially reversed by DFO and Fer-1 (Figure S1E). The FerroOrange fluorescent probe was used to detect Fe^{2+}, and the results showed that FAC further exacerbated the increase of Fe^{2+} in OS cells induced by ART (Figure 3F,G). Similarly, lipid peroxidation levels in OS cells were further increased and could be reversed by DFO and Fer-1 (Figure 3H,I). Together, these results suggested that iron overload further exacerbated ART-induced ferroptosis in OS cells.

3.4 | Fer-1 reversed ART-induced ferroptosis in OS cells

Ferroptosis was characterized by the accumulation of iron, ROS, and lipid peroxidation overload, and was negatively regulated by xCT and GPX4.[24] The levels of intracellular ROS and lipid peroxidation were measured separately using the fluorescent probe DCFH-DA and C11-BODIPY589/591, and the flow cytometry results showed that ART treatment for 24 h could significantly increase the intracellular ROS (Figure 4A,B) and lipid peroxidation (Figure 4C,D), which could be partially reversed by Fer-1. GSH and MDA are both important biomarkers in the context of ferroptosis.[25] The results showed that the GSH content decreased (Figure 4E) and the MDA content increased (Figure 4F) in OS cells after ART treatment and could be partially reversed by Fer-1. xCT and GPX4 are the key proteins of ferroptosis; western blot results showed that ART downregulated the expression of xCT and GPX4 proteins in OS cells (Figure 4G,H). Mitochondria, often referred to as the "energy generators" of cells, are essential organelles that maintain normal cellular metabolic activities.[26] Transmission electron microscopy (TEM) was used to observe the morphological changes in MG63 and 143B cells after treatment with a compound called ART for 24 h. The TEM images revealed that the treated cells exhibited several typical morphological features of ferroptosis, including mitochondrial shrinkage, a higher density of the mitochondrial membrane, and reduction or disappearance of mitochondrial cristae (indicated by red arrows) (Figure 4I).

3.5 | Inhibition of autophagy attenuated ART-induced ferroptosis in OS cells

In the transcriptome sequencing results, GO enrichment analysis showed that autophagy was also one of the pathways by which ART inhibited the activity of OS cells. In addition, autophagy inhibitor 3-MA partially reversed ART-induced inhibition of OS cell viability. We demonstrated that ART could induce autophagy in OS cells. LC3 I/II and P62 are the key proteins of autophagy; western blot analysis showed that ART could upregulate the expression of LC3 I/II protein and downregulate the expression of P62 protein in OS cells (Figure 5A,B). Subsequently, we explored the relationship between ART-induced ferroptosis and autophagy in OS cells. Interestingly, autophagy inhibitor 3-MA significantly inhibited ART-induced elevation of Fe^{2+} levels (Figure 5C,D) and lipid peroxidation accumulation (Figure 5E,F) in OS cells. Analogously, 3-MA treatment successfully reversed the expression of P62, xCT, and GPX4 proteins (Figure 5G,H). We further investigated the relationship between autophagy and the increase in Fe^{2+} levels induced by ART, as ART-induced ferroptosis in OS cells was dependent on Fe^{2+} elevation. Interestingly, treatment with an autophagy inhibitor, 3-MA (1 mM), for 24 h markedly reversed the expression levels of FTH1 protein, while the expression of TFR and DMT1 proteins did not change significantly (Figure 5I,J).

3.6 | NCOA4-mediated ferritinophagy was involved in ART-induced intracellular iron overload

Previous reports have shown that autophagy could selectively degrade ferritin through NCOA4 (namely ferritinophagy), which increases intracellular iron

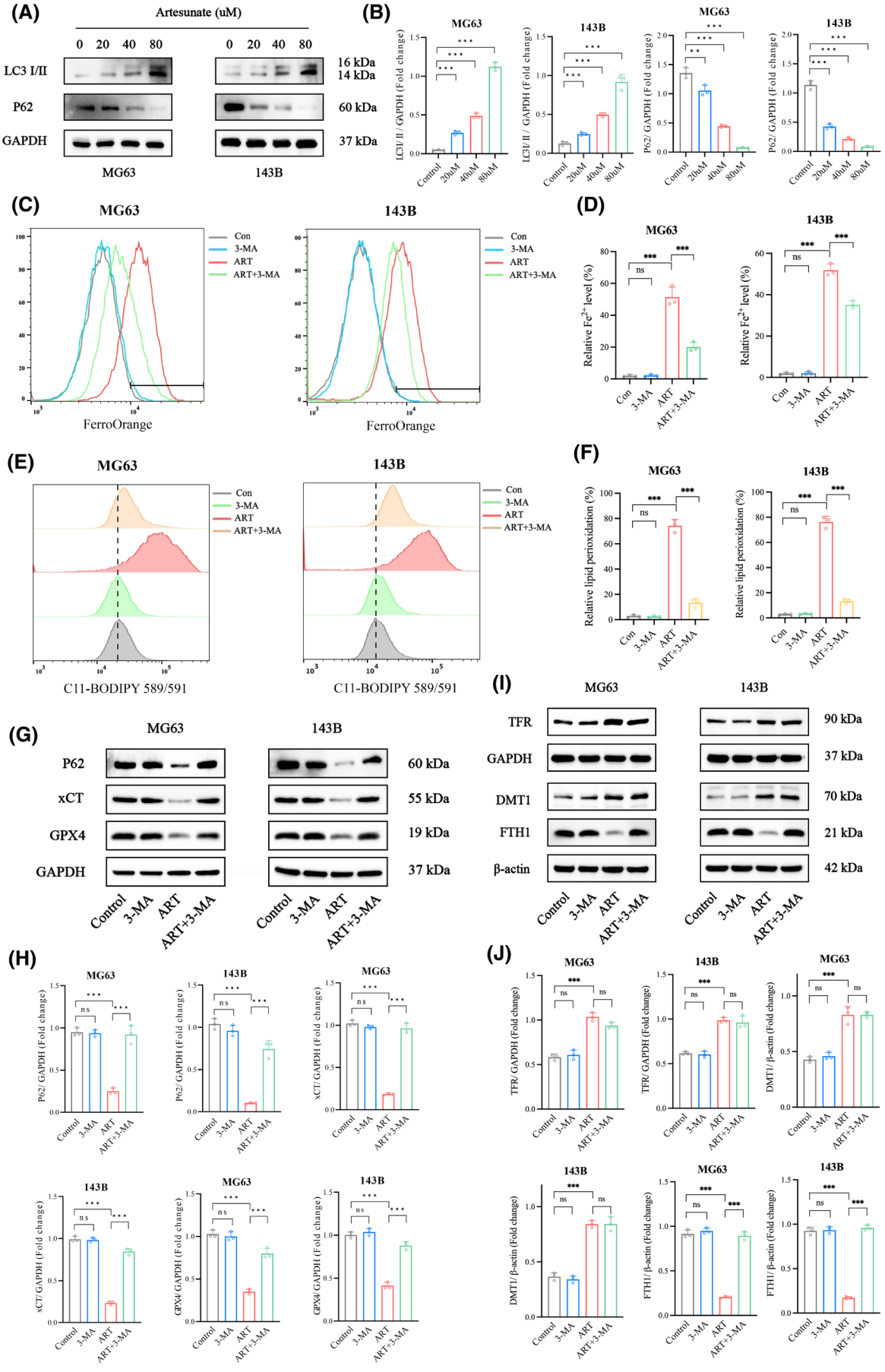
(A)
Artesunate (uM)
0 20 40 80
0 20 40 80
LC3 I/II
P62
GAPDH
16 kDa
14 kDa
60 kDa
37 kDa
MG63
143B
(B)
MG63
143B
LC3I/ II / GAPDH (Fold change)
P62/ GAPDH (Fold change)
Control
20uM
40uM
80uM
(C)
MG63
143B
Con
3-MA
ART
ART+3-MA
FerroOrange
(D)
Relative Fe2+ level (%)
(E)
C11-BODIPY 589/591
(F)
Relative lipid perioxidation (%)
(G)
P62
xCT
GPX4
GAPDH
60 kDa
55 kDa
19 kDa
37 kDa
Control
3-MA
ART
ART+3-MA
(H)
P62/ GAPDH (Fold change)
xCT/ GAPDH (Fold change)
GPX4/ GAPDH (Fold change)
(I)
TFR
GAPDH
DMT1
FTH1
β-actin
90 kDa
37 kDa
70 kDa
21 kDa
42 kDa
(J)
TFR/ GAPDH (Fold change)
DMT1/ β-actin (Fold change)
FTH1/ β-actin (Fold change)

FIGURE 5 Inhibition of autophagy attenuated ART-induced ferroptosis in OS cells. (A, B) Western blot was used to detect the expression of autophagy related protein LC3 I/II and P62, and quantification was analyzed. (C, D) Intracellular Fe^{2+} was observed by flow cytometry analysis after the intervention of ART with or without 3-MA after 24 h in MG63 and 143B cells, followed by quantitative analysis. (E, F) The lipid peroxidation was evaluated in MG63 and 143B cells after the intervention of ART with or without 3-MA after 24 h by using flow cytometry analysis with C11-BODIPY 589/591 staining, followed by quantitative analysis. (G, H) Western blot was used to detect the expression of protein P62, xCT and GPX4, and quantification was analyzed. (I, J) Western blot was used to detect the expression of protein TFR, DMT1 and FTH1, and quantification was analyzed. Data represent mean ± SD, significance in (B), (D), (F), (H) and (J) were calculated using the one-way ANOVA with Dunnett's multiple comparisons test. $n = 3$; $^{**}p < .01$; $^{***}p < .001$.

levels to promote ferroptosis.[27] In addition, we found that ART could up-regulate NCOA4 expression in a dose-dependent manner (Figure 6A,B). To further confirm whether increased NCOA4 contributed to ART-induced ferritinophagy, we established NCOA4 knockdown OS cells. The reversal of FTH1 downregulation by NCOA4 knockdown indicated that NCOA4 plays a critical role in ART-induced ferritinophagy (Figure 6C,D). By targeting ferritin for degradation, NCOA4 may contribute to the release of iron and the induction of ferroptosis. The knockdown of NCOA4 blocked this process, leading to increased FTH1 levels and potentially decreased ferroptosis. Similarly, the knockdown of NCOA4 reversed the elevated Fe^{2+} (Figure 6E) and lipid peroxidation accumulation (Figure 6F,G). These results suggested that NCOA4-mediated ferritinophagy is involved in ART-induced ferroptosis in OS cells.

3.7 | Intracellular iron overload increased mitochondrial iron levels and dysfunction

Mitochondria are the core of redox homeostasis and iron homeostasis during ferroptosis. Excessive Fe^{2+} in mitochondria could produce a large number of ROS via the Fenton reaction, which could promote ferroptosis. Mito-FerroGreen and mito-SOX fluorescent probes were used to detect the changes in Fe^{2+} and ROS levels in mitochondria of MG63 and 143B cells after ART treatment for 24 h, and the results showed that ART could increase the level of mitochondrial Fe^{2+} (Figure 7A) and ROS (Figure 7B), which could be significantly reversed by DFO. Mitochondria are the primary sites for the production of ROS. An increase in ROS levels can lead to the opening of mitochondrial permeability transition pores (MPT).[28] The opening of these pores leads to a reduction in MMP, ultimately resulting in mitochondrial damage.[29] In addition to being important indicators of mitochondrial damage and the start of ferroptosis, aberrant MMP changes are also a precursor to ferroptosis.[30] The JC-1 fluorescent probe was used to detect the changes in the MMP levels in MG63 and 143B cells after ART treatment for 24 h, and the results showed that ART reduced MMP, and membrane depolarization was reversed by DFO treatment (Figure 7C,D).

3.8 | Knockdown of Mfrn2 significantly rescued the increase in mitochondrial free iron

Mfrn1 and Mfrn2 are proteins that belong to the mitochondrial solute carrier family. They play a crucial role in transporting iron into the mitochondria. Ftmt plays a key role in maintaining iron homeostasis within the cell by binding to excess iron ions and forming ferritin complexes. This helps to prevent damage to cellular structures and functions caused by excessive iron. We found that the expression of Mfrn2 was upregulated while Ftmt was downregulated after ART treatment, which could be significantly reversed by DFO (Figure 8A,B), suggesting that the increase in mitochondrial Fe^{2+} may be the result of enhanced iron input and decreased iron storage. In addition, the knockdown of Mfrn2 significantly decreased the levels of mitochondrial free iron and mitochondrial ROS (Figure 8C–F). All of these findings showed that mitochondrial iron levels and dysfunction were elevated by cytosolic iron overload brought on by ART.

3.9 | ART suppressed the tumor growth in vivo by inducing ferroptosis

To further confirm the anti-OS effects of ART in vivo, an orthotopic intra-tibia tumor-bearing model was established, and ART was administered via daily intraperitoneal injections. The results indicated that ART treatment did not significantly affect the body weight of the mice, while the tumor volume in the treatment group was significantly reduced compared to the control group (Figure 9A–D). These suppressive effects were partially antagonized by the Fer-1 administration. To further explore the potential toxicity of ART, the biochemical parameters of the liver and kidney in mice were assessed, and the results showed that ART had no obvious toxic effect on the liver and kidney of the mice (Figure 9E–H). Hematoxylin and eosin (HE) staining

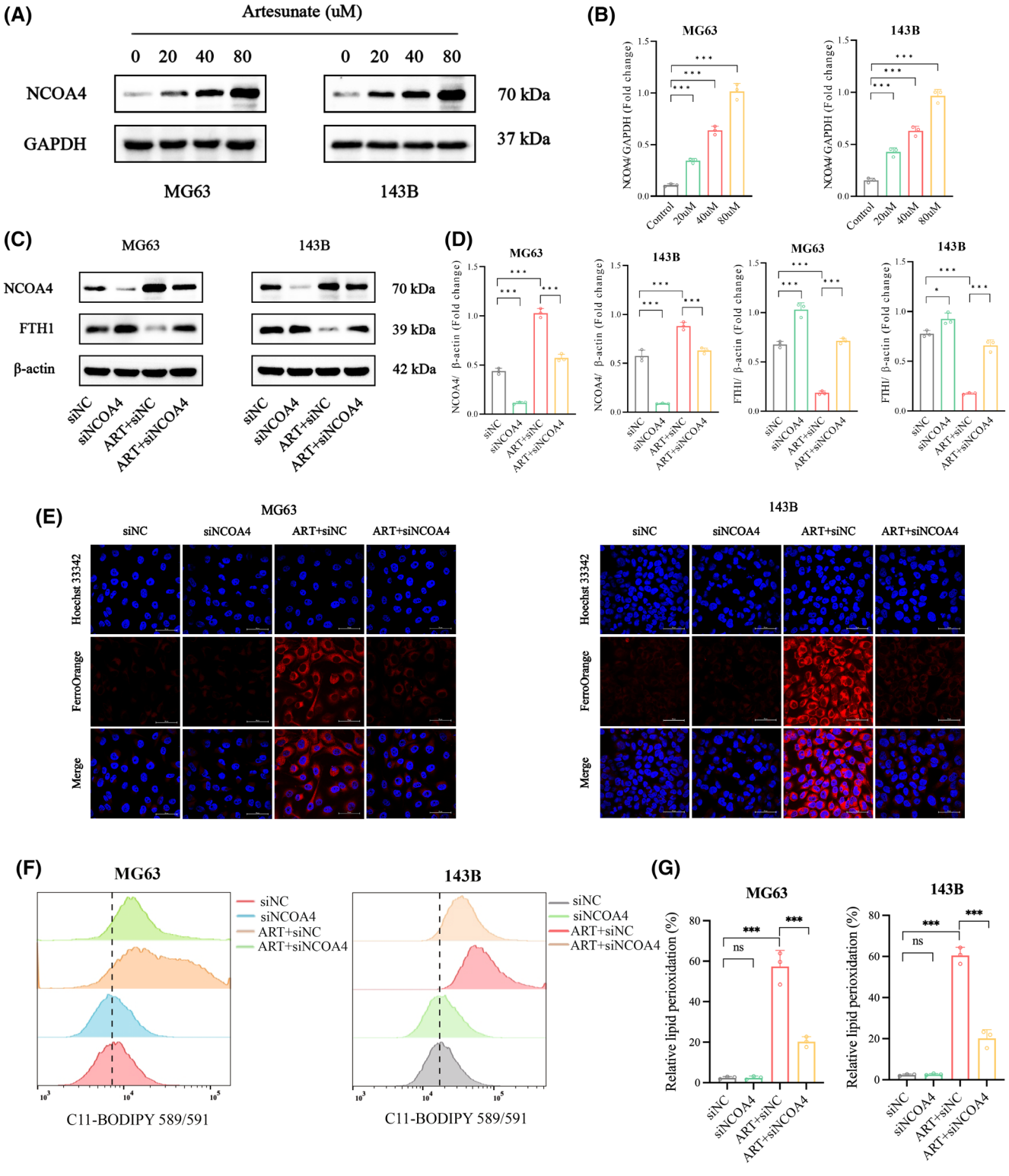

FIGURE 6 NCOA4-mediated ferritinophagy was involved in ART-induced intracellular iron overload. (A, B) Western blot was used to detect the expression of protein NCOA4; quantification was analyzed. (C, D) Western blot was used to detect the expression of protein NCOA4 and FTH1 after the intervention of ART with or without siNCOA4; quantification was analyzed. (E) Intracellular Fe^{2+} was observed by using LSCM after the intervention of ART with or without siNCOA4 after 24 h in MG63 and 143B cells (scale bar: 50 μm). (F, G) The lipid peroxidation was evaluated in MG63 and 143B cells after the intervention of ART with or without siNCOA4 after 24 h by using flow cytometry analysis with C11-BODIPY 589/591 staining, followed by quantitative analysis. Data represent mean ± SD; significance in (B), (D) and (G) was calculated using the one-way ANOVA with Dunnett's multiple comparisons test. $n = 3$; $^{*}p < .05$; $^{***}p < .001$.

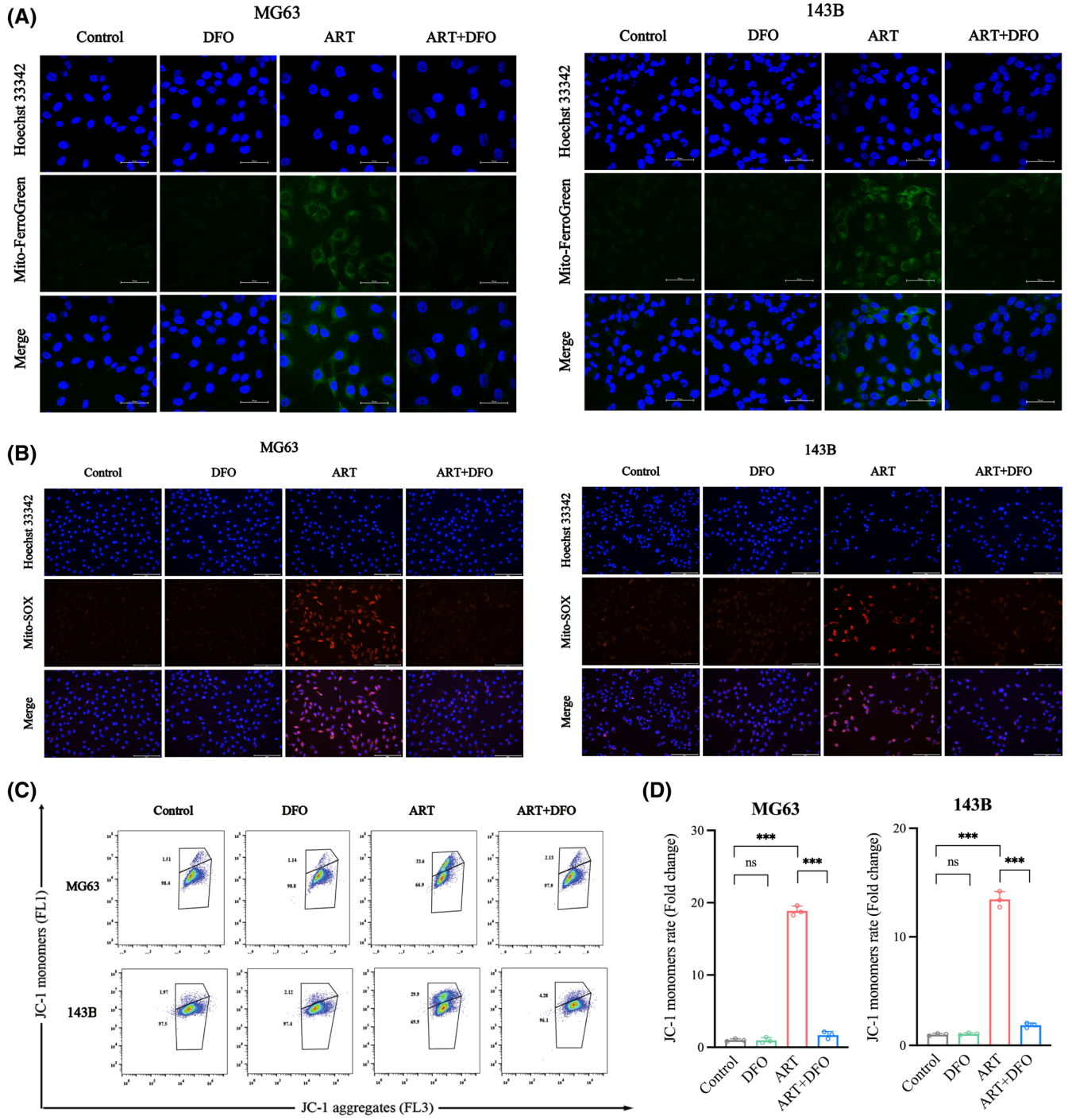

FIGURE 7 Intracellular iron overload increased mitochondrial iron levels and dysfunction. (A) Mitochondrial Fe^{2+} was observed by Mito-FerroGreen staining after the intervention of ART with or without DFO after 24 h in OS cells, followed by quantitative analysis (scale bar: 50 μm). (B) Mitochondrial ROS contents were observed by using Mito-SOX staining after the intervention of ART with or without DFO after 24 h in OS cells, followed by quantitative analysis (scale bar: 100 μm). (C, D) Flow cytometry scatter plot of JC-1 MMP detection, showing the distribution of MG63 and 143B cells based on fluorescence intensity. Green fluorescence (FL1) is represented on the y-axis, while red fluorescence (FL3) is represented on the x-axis. Data represent mean ± SD; significance in (D) was calculated using the one-way ANOVA with Dunnett's multiple comparisons test. $n = 3$; ***$p < .001$.

also demonstrated that ART significantly inhibited the growth of metastatic lung tumors, while Fer-1 administration notably diminished this inhibitory effect (Figure 9I). Moreover, the results of immunohistochemical staining indicated that ART administration could upregulate the expression of NCOA4 and downregulate the expression of Ki67 and GPX4, which were sharply reversed by Fer-1 administration (Figure 9J). These results suggested that

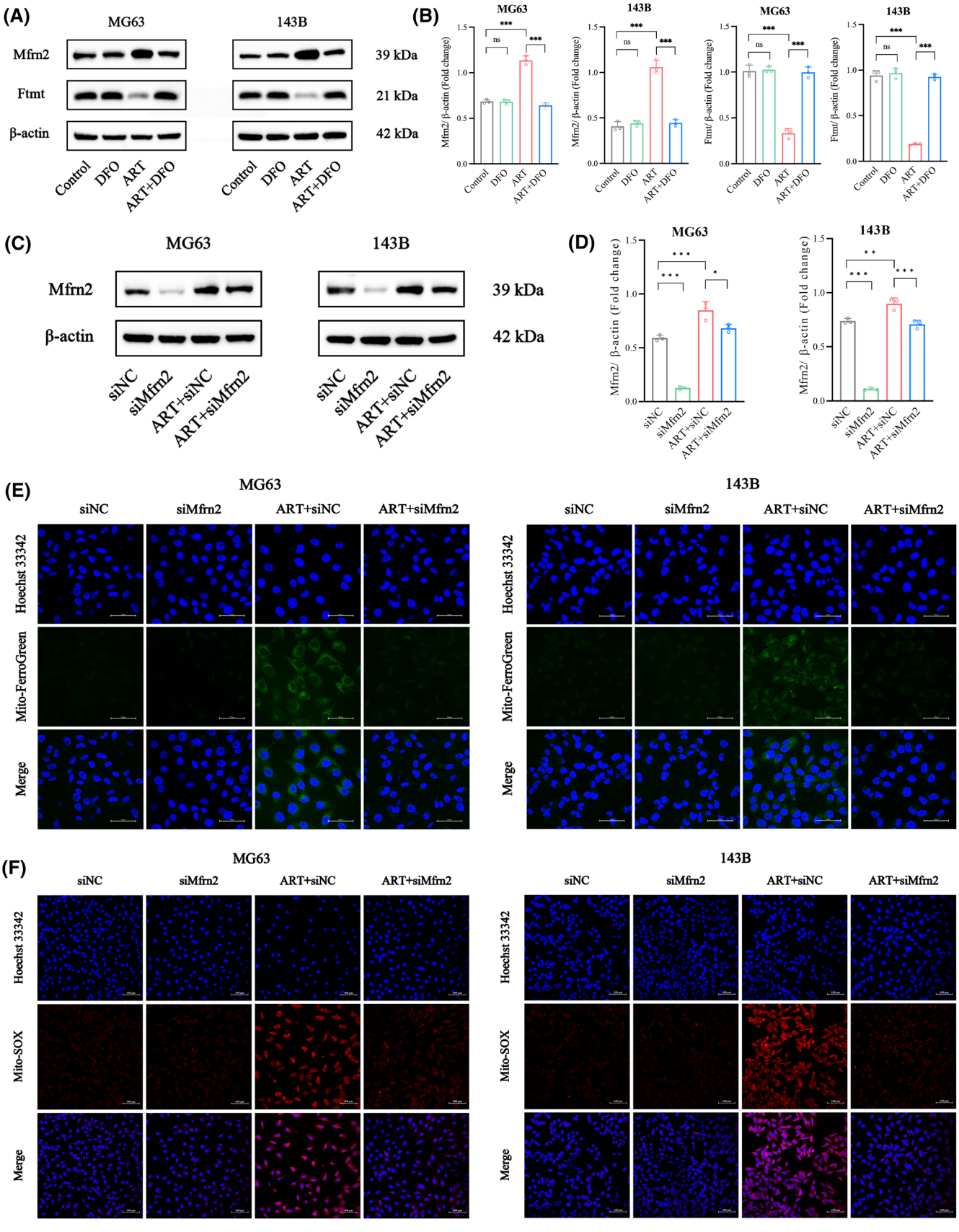
(A)
MG63
143B
Mfrn2
Ftmt
β-actin
39 kDa
21 kDa
42 kDa
Control
DFO
ART
ART+DFO
(B)
MG63
143B
Mfrn2/ β-actin (Fold change)
Ftmt/ β-actin (Fold change)
ns
***
(C)
MG63
143B
Mfrn2
β-actin
39 kDa
42 kDa
siNC
siMfrn2
ART+siNC
ART+siMfrn2
(D)
MG63
143B
Mfrn2/ β-actin (Fold change)
(E)
MG63
143B
siNC
siMfrn2
ART+siNC
ART+siMfrn2
Hoechst 33342
Mito-FerroGreen
Merge
(F)
MG63
143B
siNC
siMfrn2
ART+siNC
ART+siMfrn2
Hoechst 33342
Mito-SOX
Merge

FIGURE 8 Knockdown of Mfrn2 significantly rescued the increase in mitochondrial free iron. (A, B) Western blot was used to detect the expression of Mfrn2 and Ftmt after the intervention of ART with or without DFO, quantification was analyzed. (C, D) Western blot was used to detect the expression of Mfrn2 after the intervention of ART with or without siMfrn2, quantification was analyzed. (E) Mitochondrial Fe^{2+} were observed after the intervention of ART with or without siMfrn2, followed by quantitative analysis, (scale bar: 50 μm). (F) Mitochondrial ROS contents were observed after the intervention of ART with or without siMfrn2, followed by quantitative analysis (scale bar: 100um). Data represent mean ± SD, significance in (B) and (D) were calculated using the one-way ANOVA with Dunnett's multiple comparisons test. $n = 3$; $^{*}p < .05$; $^{**}p < .01$; $^{***}p < .001$.

ART inhibited the growth of OS through the ferroptosis pathway in vivo.

4 | DISCUSSION

OS has been the most common primary malignant bone tumor in children and adolescents.[31] Due to the high degree of malignancy of OS, the toxicity of effective therapeutic doses of first-line anti-cancer drugs, and multi-drug resistance, chemotherapy for OS faces significant challenges.[18] Therefore, it is urgent to explore new therapeutic targets and develop effective anti-OS drugs. ART is a more potent derivative of artemisinin, which has many pharmacological activities such as anti-malarial, anti-inflammatory, and anti-tumor. However, further elucidation of the target and mechanism of pharmacological action is essential for its development as an anticancer drug. In this study, we presented significant evidence supporting the effective anti-OS activity of ART both in vitro and in vivo, markedly inhibiting proliferation rates and inducing cell cycle arrest in a dose-dependent manner. Subsequently, the potential anti-OS mechanism of ART was discussed from the perspective of regulating the cell death subroutine. Notably, ferroptosis may be a critical pathway for ART to treat OS. Mechanistically, on the one hand, ART induced NCOA4-mediated ferritinophagy, leading to FTH1 degradation and iron release; on the other hand, ART upregulated the expression of TFR and DMT1. These factors jointly increased the level of intracellular Fe^{2+} and activated Mfrn2 on the mitochondrial membrane. Mfrn2-mediated transport of cytoplasmic free iron into the mitochondria results in mitochondrial iron overload and excessive ROS production, eventually leading to lipid peroxidation and ferroptosis. In summary, these findings suggested that ART induced ferroptosis by promoting NCOA4-mediated ferritinophagy, which exerted its anti-OS effects, potentially providing new insights into the therapeutic applications of ART in diseases related to oxidative stress and iron metabolism.

As a novel mode of PCD, ferroptosis is involved in the development and treatment of many diseases.[18,32] The recent interest in determining the critical role of ferroptosis in malignancy inhibition is increasing.[33] For example, Polyphyllin I induced ferroptosis to suppress the progression of hepatocellular carcinoma via the Nrf2/HO-1/GPX4 axis.[34] Ginkgetin enhanced the therapeutic effect of cisplatin via ferroptosis in EGFR wild-type non-small-cell lung cancer.[35] Therefore, ferroptosis is a promising therapeutic strategy for inhibiting cancer progression. In the present study, transcriptome sequencing showed that ferroptosis is one of the most important ways of ART action on OS cells. Subsequently, we combined multiple cell death pathway inhibitors to conduct rescue experiments and found that ferroptosis inhibitors Fer-1 and DFO could significantly reverse the inhibitory effect of ART on OS cells. In addition, intracellular Fe^{2+} content, ROS, and lipid peroxidation levels increased after treatment with ART, and these could be rescued by Fer-1. The morphological changes of OS cells treated with ART were also consistent with ferroptosis, implying that ART could cause ferroptosis in OS cells. Intracellular iron homeostasis is essential for cell survival, and the disturbance of intracellular iron metabolism, especially the increase of Fe^{2+} content, is the initial factor of ferroptosis.[36] Moreover, when iron overload in tumor cells leads to excess ROS production through the Fenton reaction, it promotes ferroptosis and tumor inhibition.[18] Triggering lipid peroxidation, defined as the programmed process by which ROS strongly attack polyunsaturated fatty acids, is the canonical event that drives ferroptosis.[37] In this study, we found that ART-mediated iron accumulation primarily contributes to ferroptosis in OS cells.

NCOA4 functions as a cargo receptor that specifically targets ferritin within the autophagosome during the process of selective autophagy.[38] NCOA4-mediated ferritinophagy increases intracellular Fe^{2+} content by degrading ferritin, resulting in the upregulation of NCOA4 and the degradation of FTH1. This, in turn, triggers the accumulation of iron. In this study, we made an intriguing discovery that ART induced autophagy in OS cells, and subsequently we explored the relationship between ART-induced ferroptosis and autophagy, finding that the inhibition of autophagy weakened ferroptosis. Interestingly, our findings indicated that the silencing of NCOA4 effectively reversed the ferroptosis induced by ART in OS cells, thereby suggesting that NCOA4 was essential for this process. Furthermore, an additional mechanism through

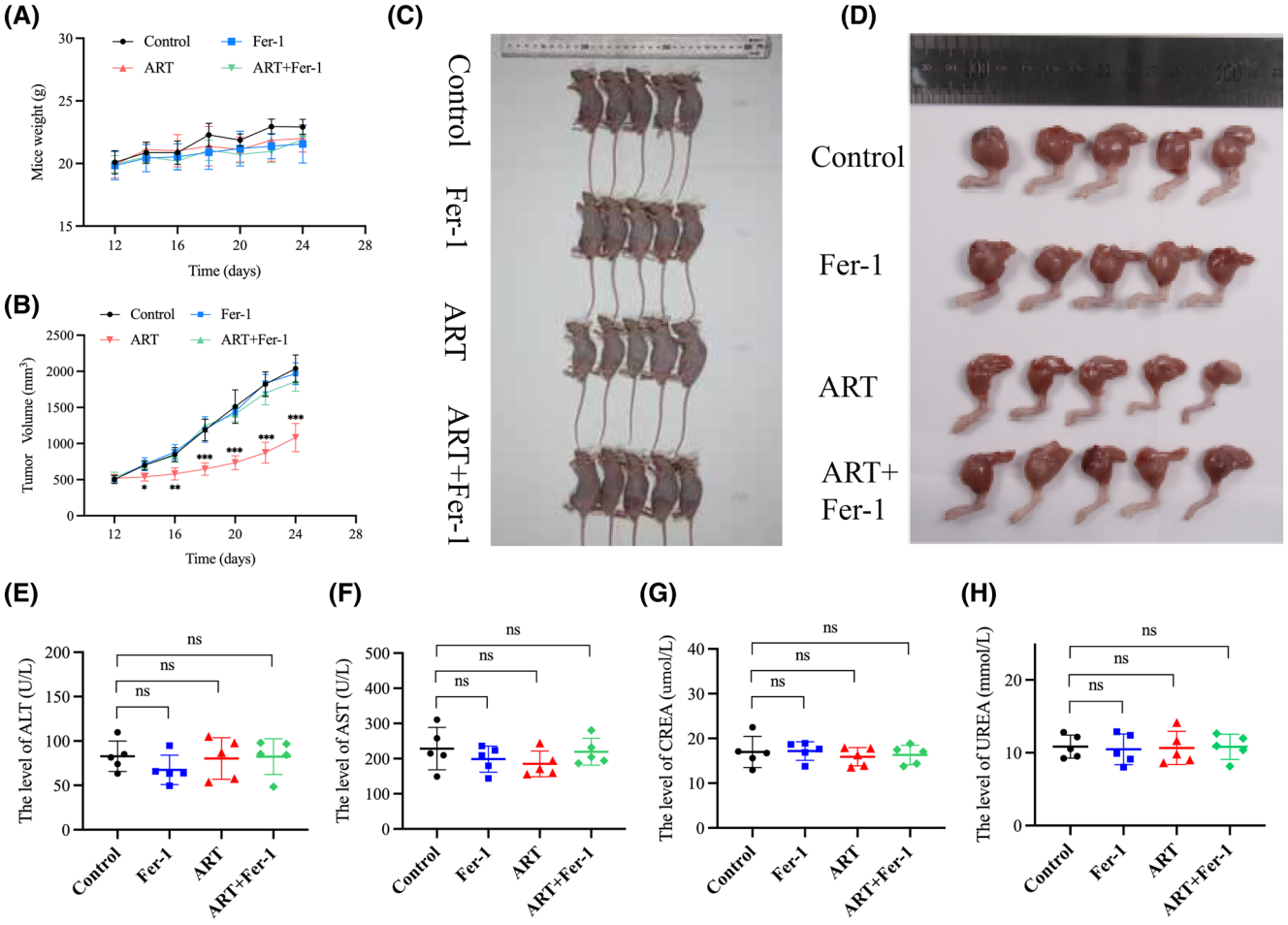
(A)
Control
Fer-1
ART
ART+Fer-1
Mice weight (g)
Time (days)
(B)
Tumor Volume (mm3)
(C)
Control
Fer-1
ART
ART+Fer-1
(D)
(E)
The level of ALT (U/L)
(F)
The level of AST (U/L)
(G)
The level of CREA (umol/L)
(H)
The level of UREA (mmol/L)
ns

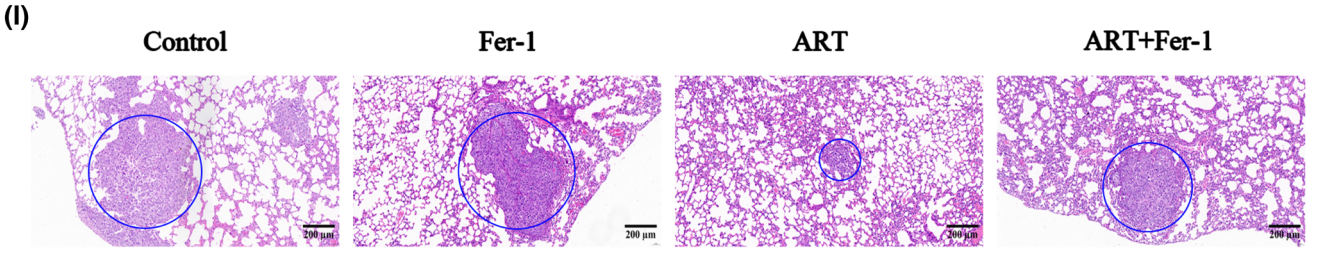
(I)
Control
Fer-1
ART
ART+Fer-1
200 μm

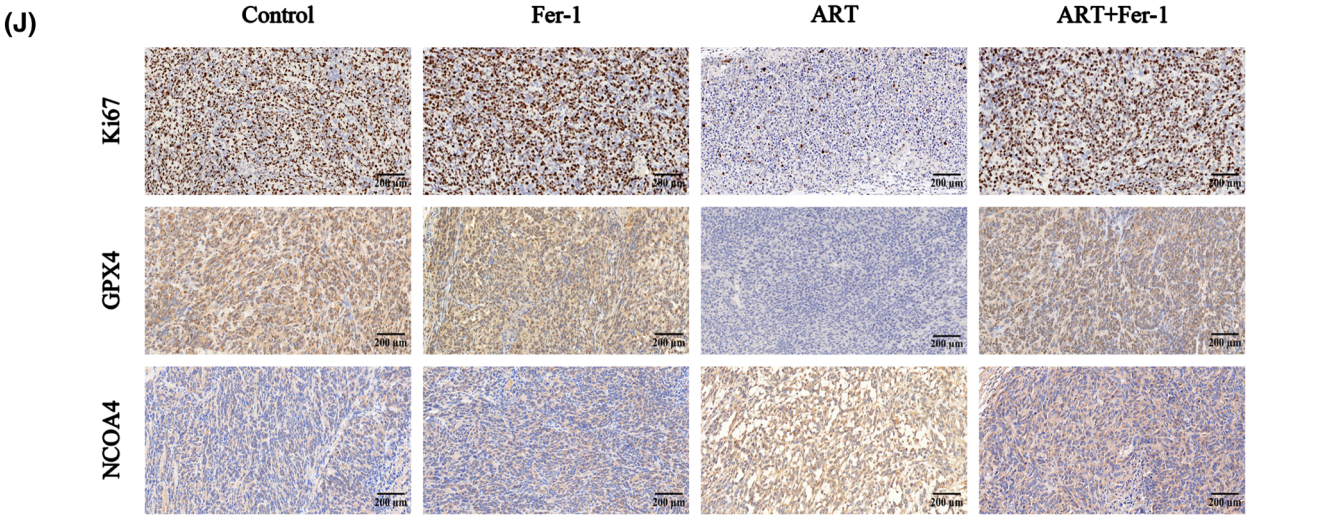
(J)
Control
Fer-1
ART
ART+Fer-1
Ki67
GPX4
NCOA4
200 μm

FIGURE 9 ART suppressed the tumor growth in vivo through inducing ferroptosis. (A, B) The growth curve of tumor volumes and tumor weights were examined in the animals treated with control, ART, Fer-1 or Fer-1 + ART respectively. (C-D) The representative images of burdened tumors in each group. (E–H) The level of ALT (E), AST (F), CREA (G) and UREA (H) were measured in each group. (I) HE staining for the lung tissue in each group, (scale bar: 200 μm). (J) The immunohistochemical analyses of Ki67, GPX4 and NCOA4 were examined in tumor tissues, (scale bar: 200 μm). Data represent mean ± SD, Significance in (A), (B) and (E–H) were calculated using the one-way ANOVA with Dunnett's multiple comparisons test. $n = 5$; *$p < .05$; **$p < .01$; ***$p < .001$; ns, no significant.

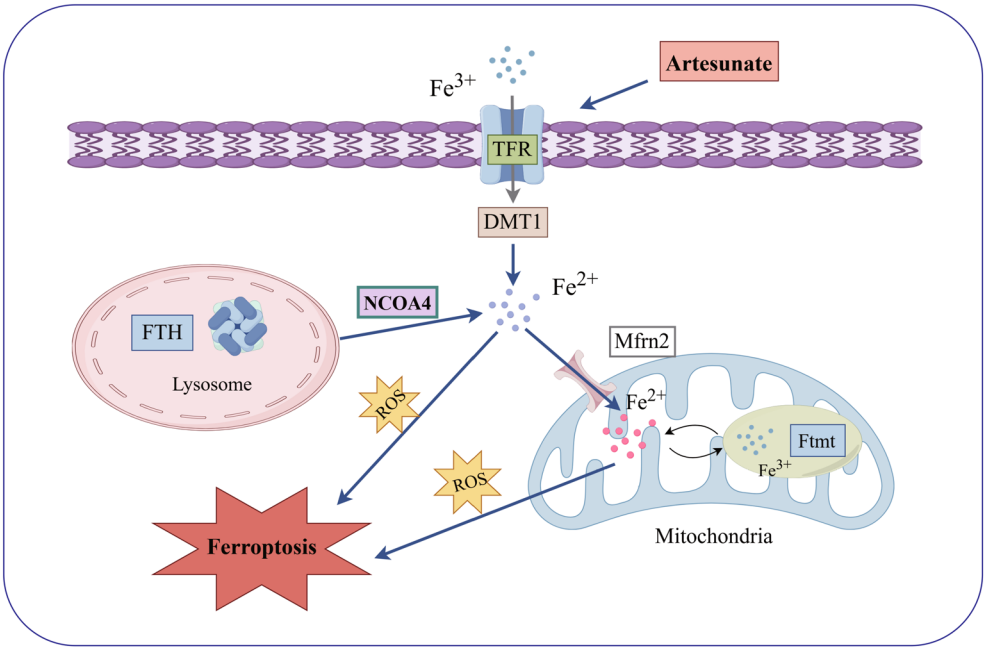

FIGURE 10 Schematic illustration of the molecular mechanism for ART-induced ferroptosis of OS cells.

which ART elevated Fe^{2+} levels in OS cells involved the upregulation of TFR protein expression. The main route for iron ions to enter cells is through the TF/TFR-1 transport system, and the presence of these channels and transport systems allows iron ions to be absorbed and utilized by cells. Similar to TFR, DMT1 is also a positive regulator of iron accumulation, leading to ferroptosis.[39] We found that ART treatment increased the expression of TFR and DMT1, which, together with the degradation of FTH1, promoted the increase of intracellular Fe^{2+}, thereby increasing the level of intracellular lipid peroxidation and triggering ferroptosis in OS cells.

xCT, a crucial component in the process of ferroptosis, is a cystine/glutamate antiporter responsible for exporting glutamate and importing cysteine.[40] GPX4, a selenoprotein belonging to the glutathione peroxidase family, is a central regulator of ferroptosis that prevents ROS accumulation and reduces hydroperoxides, rescuing cell membranes from lipid peroxidation damage.[41] As previously reported, GPX4 is an important negative regulator of ferroptosis, and the inhibition of GPX4 triggers ferroptosis.[42] A previous study showed that ART inhibits the growth of insulinoma cells via SLC7A11/GPX4-mediated ferroptosis.[43] In the present study, our results demonstrated that the expression of xCT and GPX4 was suppressed by ART in OS cells, and this suppression could be rescued by the ferroptosis inhibitor Fer-1.

Mitochondria are the "energy generators" of cellular metabolic activities, and mitochondrial damage and morphological changes are usually the early events of cell death.[44] Compared with other types of PCD, ferroptosis has special mitochondrial morphological changes.[45] In this study, we found that the mitochondrial morphology following ART treatment was consistent with the classical characteristics of ferroptosis, and the MMP decreased. Interestingly, ART-induced mitochondrial damage was alleviated when the endogenous Fe^{2+} was chelated by DFO. In addition, mitochondria are the primary organelles that regulate iron homeostasis in cells.[46] In eukaryotic cells, cytosolic free Fe^{2+} is transported into the mitochondria for heme and iron–sulfur (Fe/S) cluster synthesis.[47] Mitochondria are the main sites of ROS production and are closely related to the occurrence of ferroptosis.[48] Consistent with this, we found that the accumulation of Fe^{2+} and ROS in mitochondria induced by ART in OS cellscould be rescued by DFO. Mitochondria are responsible for the import

and storage of iron, facilitated by the Mfrn2 and Ftmt proteins, respectively.[49] In this study, the expression of Mfrn2 and Ftmt was elevated after ART treatment and could be reversed by DFO. Interestingly, when we silenced Mfrn2 expression, the ART-induced elevation of mitochondrial Fe^{2+} and ROS was markedly reduced. These results suggest that Mfrn2 plays an important role in ART-induced ferroptosis in OS cells.

5 | CONCLUSION

In conclusion, our findings demonstrate that ART has exerted anti-OS effects in vitro and in vivo by triggering ferroptosis. Mechanistically, ART triggers ferritinophagy by upregulating the expression of NCOA4, thereby leading to FTH1 degradation and ultimately inducing ferroptosis in OS cells, as shown in Figure 10. These findings provide novel insights into the function of ART in promoting ferroptosis in OS cells and reaffirm its potential as a promising pharmaceutical for the treatment of OS.

AUTHOR CONTRIBUTIONS

Conceptualization, formal analysis, investigation, resources, supervision, writing–original draft, writing–review and editing: Rui Huang. *Investigation, Methodology, Data curation, project administration, resources, writing–original draft*: Ruiqing Xu. *Conceptualization, formal analysis, investigation, supervision, writing–original draft*: Jiandang Shi. *Data curation, formal analysis, investigation, methodology, visualization, writing–original draft*: Zongqiang Yang. *Writing–original draft, data curation, formal analysis, investigation, methodology, visualization*: Jianping Zheng and Daihao Wei.

ACKNOWLEDGMENTS

We thank the Science and Technology Center of Ningxia Medical University for providing support for this study.

FUNDING INFORMATION

This work was supported by the Key Program of Ningxia Hui Autonomous Region Natural Science Foundation of China (No. 2024AAC02069) and the Program of Ningxia Hui Autonomous Region Natural Science Foundation (No. 2024AAC03573).

DISCLOSURES

The authors declare no conflicts of interest.

DATA AVAILABILITY STATEMENT

The data that support the findings of this study are available in the Materials and Methods, Results, and/or Supplemental Material of this article.

ORCID

Rui Huang https://orcid.org/0000-0003-0619-9666
Ruiqing Xu https://orcid.org/0009-0002-3932-2122
Jiandang Shi https://orcid.org/0000-0003-1239-1822
Zongqiang Yang https://orcid.org/0000-0002-2773-1175
Jianping Zheng https://orcid.org/0000-0003-0086-0935
Daihao Wei https://orcid.org/0009-0000-0242-9482

REFERENCES

1. Li HB, Huang G, Tu J, et al. METTL14-mediated epitranscriptome modification of MN1 mRNA promote tumorigenicity and all-trans-retinoic acid resistance in osteosarcoma. *EBioMedicine*. 2022;82:104142. doi:10.1016/j.ebiom.2022.104142
2. Yu T, Jiang W, Wang Y, Zhou Y, Jiao J, Wu M. Chimeric antigen receptor T cells in the treatment of osteosarcoma (review). *Int J Oncol*. 2024;64(4):40. doi:10.3892/ijo.2024.5628
3. Wang S, Lin B, Liu W, et al. Acacetin induces apoptosis in human osteosarcoma cells by modulation of ROS/JNK activation. *Drug Des Devel Ther*. 2020;14:5077-5085. doi:10.2147/DDDT.S275148
4. Mace KE, Lucchi NW, Tan KR. Malaria Surveillance—United States, 2017. *MMWR Surveill Summ*. 2021;70(2):1-35. doi:10.15585/mmwr.ss7002a1
5. Luo H, Vong CT, Chen H, et al. Naturally occurring anti-cancer compounds: shining from chinese herbal medicine. *Chin Med*. 2019;14:48. doi:10.1186/s13020-019-0270-9
6. Salahuddin N, Gaber M, Mousa M, Elfiky M. Dopamine/artesunate loaded polyhydroxybutyrate-g-cellulose- magnetite zinc oxide core shell nanocomposites: synergistic antimicrobial and anticancer efficacy. *Int J Biol Macromol*. 2023;248:125348. doi:10.1016/j.ijbiomac.2023.125348
7. Chen SY, Chao CN, Huang HY, Zhao PW, Fang CY. Artesunate exhibits synergy with cisplatin and cytotoxicity for upper tract and bladder urothelial carcinoma cells. *Anticancer Res*. 2023;43(3):1175-1184. doi:10.21873/anticanres.16263
8. Li ZJ, Dai HQ, Huang XW, et al. Artesunate synergizes with sorafenib to induce ferroptosis in hepatocellular carcinoma. *Acta Pharmacol Sin*. 2021;42(2):301-310. doi:10.1038/s41401-020-0478-3
9. Wang JS, Wang MJ, Lu X, et al. Artesunate inhibits epithelial-mesenchymal transition in non-small-cell lung cancer (NSCLC) cells by down-regulating the expression of BTBD7. *Bioengineered*. 2020;11(1):1197-1207. doi:10.1080/21655979.2020.1834727
10. Yu H, Gong M, Qi J, et al. Systematic transcriptome profiling of pyroptosis related signature for predicting prognosis and immune landscape in lower grade glioma. *BMC Cancer*. 2022;22(1):885. doi:10.1186/s12885-022-09982-7
11. Dong W, Zhang H, Han L, et al. Revealing prognostic insights of programmed cell death (PCD)-associated genes in advanced non-small cell lung cancer. *Aging (Albany NY)*. 2024;16(9):8110-8141. doi:10.18632/aging.205807
12. Chen X, Li J, Kang R, Klionsky DJ, Tang D. Ferroptosis: machinery and regulation. *Autophagy*. 2021;17(9):2054-2081. doi:10.1080/15548627.2020.1810918
13. Cheng Z, Li Z, Gu L, et al. Ophiopogonin b alleviates cisplatin resistance of lung cancer cells by inducing caspase-1/

GSDMD dependent pyroptosis. *J Cancer*. 2022;13(2):715-727. doi:10.7150/jca.66432

14. Zhai FG, Liang QC, Wu YY, Liu JQ, Liu JW. Red ginseng polysaccharide exhibits anticancer activity through GPX4 downregulation-induced ferroptosis. *Pharm Biol*. 2022;60(1):909-914. doi:10.1080/13880209.2022.2066139
15. Liu Y, Liu X, Wang H, Ding P, Wang C. Agrimonolide inhibits cancer progression and induces ferroptosis and apoptosis by targeting SCD1 in ovarian cancer cells. *Phytomedicine*. 2022;101:154102. doi:10.1016/j.phymed.2022.154102
16. Yang C, Lu T, Liu M, et al. Tiliroside targets TBK1 to induce ferroptosis and sensitize hepatocellular carcinoma to sorafenib. *Phytomedicine*. 2023;111:154668. doi:10.1016/j.phymed.2023.154668
17. Wu Y, Pi D, Zhou S, et al. Ginsenoside rh3 induces pyroptosis and ferroptosis through the stat3/p53/NRF2 axis in colorectal cancer cells. *Acta Biochim Biophys Sin Shanghai*. 2023;55(4):587-600. doi:10.3724/abbs.2023068
18. Huang R, Chu D, Shi J, Xu R, Wang K. Shikonin suppresses proliferation of osteosarcoma cells by inducing ferroptosis through promoting Nrf2 ubiquitination and inhibiting the xCT/GPX4 regulatory axis. *Front Pharmacol*. 2024;15:1490759. doi:10.3389/fphar.2024.1490759
19. Liang L, Liu Y, Wu X, Chen Y. Artesunate induces ferroptosis by inhibiting the nuclear localization of SREBP2 in myeloma cells. *Int J Med Sci*. 2023;20(12):1535-1550. doi:10.7150/ijms.86409
20. Bartosh UI, Dome AS, Zhukova NV, Karitskaya PE, Stepanov GA. CRISPR/cas9 as a new antiviral strategy for treating hepatitis viral infections. *Int J Mol Sci*. 2023;25(1):334. doi:10.3390/ijms25010334
21. Yu H, Liu Q, Jin M, Huang G, Cai Q. Comprehensive analysis of mitophagy-related genes in NSCLC diagnosis and immune scenery: based on bulk and single-cell RNA sequencing data. *Front Immunol*. 2023;14:1276074. doi:10.3389/fimmu.2023.1276074
22. Liu Q, Lv L, Cai X, et al. Correlation between RNA n6-methyladenosine and ferroptosis in cancer: current status and prospects. *Front Cell Dev Biol*. 2024;12:1252064. doi:10.3389/fcell.2024.1252064
23. Pan C, Zhao H, Cai X, Wu M, Qin B, Li J. The connection between autophagy and ferroptosis in AKI: recent advances regarding selective autophagy. *Ren Fail*. 2024;46(2):2379601. doi :10.1080/0886022X.2024.2379601
24. Wei S, Bi J, Yang L, et al. Serum irisin levels are decreased in patients with sepsis, and exogenous irisin suppresses ferroptosis in the liver of septic mice. *Clin Transl Med*. 2020;10(5):e173. doi:10.1002/ctm2.173
25. Han Z, Batudeligen, Chen H, et al. Luteolin attenuates CCl4-induced hepatic injury by inhibiting ferroptosis via SLC7a11. *BMC Complement Med Ther*. 2024;24(1):193. doi:10.1186/s12906-024-04486-2
26. Machihara K, Oki S, Maejima Y, et al. Restoration of mitochondrial function by spirulina polysaccharide via upregulated SOD2 in aging fibroblasts. *iScience*. 2023;26(7):107113. doi:10.1016/j.isci.2023.107113
27. Jaeschke H, Ramachandran A, Chao X, Ding WX. Emerging and established modes of cell death during acetaminophen-induced liver injury. *Arch Toxicol*. 2019;93(12):3491-3502. doi:10.1007/s00204-019-02597-1
28. Liu S, Pan Y, Li T, et al. The role of regulated programmed cell death in osteoarthritis: from pathogenesis to therapy. *Int J Mol Sci*. 2023;24(6):5364. doi:10.3390/ijms24065364
29. Rezaei M, Karimian L, Shafaghi B, et al. Evaluation of molecular and cellular alterations induced by neuropathic pain in rat brain glial cells. *Iran J Pharm Res*. 2021;20(1):359-370. doi:10.22037/ijpr.2020.113052.14089
30. Cao G, Zeng Y, Zhao Y, et al. H2s regulation of ferroptosis attenuates sepsis-induced cardiomyopathy. *Mol Med Rep*. 2022;26(5):335. doi:10.3892/mmr.2022.12851
31. Qin S, Wang X, Han P, et al. LRP1-mediated endocytosis may be the main reason for the difference in cytotoxicity of curcin and curcin C on U2OS osteosarcoma cells. *Toxins*. 2022;14(11):771. doi:10.3390/toxins14110771
32. Kontoghiorghes GJ. Iron load toxicity in medicine: from molecular and cellular aspects to clinical implications. *Int J Mol Sci*. 2023;24(16):12928. doi:10.3390/ijms241612928
33. Liang S, Bai YM, Zhou B. Identification of key ferroptosis genes and mechanisms associated with breast cancer using bioinformatics, machine learning, and experimental validation. *Aging (Albany NY)*. 2024;16(2):1781-1795. doi:10.18632/aging.205459
34. Yang R, Gao W, Wang Z, et al. Polyphyllin I induced ferroptosis to suppress the progression of hepatocellular carcinoma through activation of the mitochondrial dysfunction via Nrf2/HO-1/GPX4 axis. *Phytomedicine*. 2024;122:155135. doi:10.1016/j.phymed.2023.155135
35. Lou JS, Zhao LP, Huang ZH, et al. Ginkgetin derived from ginkgo biloba leaves enhances the therapeutic effect of cisplatin via ferroptosis-mediated disruption of the Nrf2/HO-1 axis in EGFR wild-type non-small-cell lung cancer. *Phytomedicine*. 2021;80:153370. doi:10.1016/j.phymed.2020.153370
36. Kang J, Tian S, Zhang L, Yang G. Ferroptosis in early brain injury after subarachnoid hemorrhage: review of literature. *Chin Neurosurg J*. 2024;10(1):6. doi:10.1186/s41016-024-00357-4
37. Mo X, Hu D, Yuan K, Luo J, Huang C, Xu M. Tetrandrine citrate suppresses lung adenocarcinoma growth via SLC7a11/GPX4-mediated ferroptosis. *Discov Oncol*. 2023;14(1):85. doi:10.1007/s12672-023-00691-6
38. Fujii J, Homma T, Osaki T. Superoxide radicals in the execution of cell death. *Antioxidants (Basel)*. 2022;11(3):501. doi:10.3390/antiox11030501
39. Tang D, Chen X, Kang R, Kroemer G. Ferroptosis: molecular mechanisms and health implications. *Cell Res*. 2021;31(2):107-125. doi:10.1038/s41422-020-00441-1
40. Li Y, Yang Y, Yang Y. Multifaceted roles of ferroptosis in lung diseases. *Front Mol Biosci*. 2022;9:919187. doi:10.3389/fmolb.2022.919187
41. Zhang Z, Tan Y, Huang C, Wei X. Redox signaling in drug-tolerant persister cells as an emerging therapeutic target. *EBioMedicine*. 2023;89:104483. doi:10.1016/j.ebiom.2023.104483
42. Lei P, Bai T, Sun Y. Mechanisms of ferroptosis and relations with regulated cell death: a review. *Front Physiol*. 2019;10:139. doi:10.3389/fphys.2019.00139
43. Chen F, Lu J, Zheng B, et al. Artesunate inhibits the growth of insulinoma cells via SLC7a11/GPX4-mediated ferroptosis. *Curr Pharm Des*. 2024;30(3):230-239. doi:10.2174/0113816128289372240105041038
44. Koenig AM, Liu B, Hu J. Visualizing the dynamics of plant energy organelles. *Biochem Soc Trans*. 2023;51(6):2029-2040. doi:10.1042/BST20221093

45. Wu Z, Fang ZX, Hou YY, et al. Review of ferroptosis in colorectal cancer: friends or foes? *World J Gastroenterol*. 2023;29(3):469-486. doi:10.3748/wjg.v29.i3.469
46. Akiyama H, Carter BZ, Andreeff M, Ishizawa J. Molecular mechanisms of ferroptosis and updates of ferroptosis studies in cancers and leukemia. *Cells*. 2023;12(8):1128. doi:10.3390/cells12081128
47. Karmi O, Marjault HB, Bai F, et al. A VDAC1-mediated NEET protein chain transfers [2Fe-2S] clusters between the mitochondria and the cytosol and impacts mitochondrial dynamics. *Proc Natl Acad Sci USA*. 2022;119(7):e2121491119. doi:10.1073/pnas.2121491119
48. Zhang S, Xin W, Anderson GJ, et al. Double-edge sword roles of iron in driving energy production versus instigating ferroptosis. *Cell Death Dis*. 2022;13(1):40. doi:10.1038/s41419-021-04490-1
49. Chi H, Li B, Wang Q, et al. Opportunities and challenges related to ferroptosis in glioma and neuroblastoma. *Front Oncol*. 2023;13:1065994. doi:10.3389/fonc.2023.1065994

SUPPORTING INFORMATION

Additional supporting information can be found online in the Supporting Information section at the end of this article.

How to cite this article: Huang R, Xu R, Shi J, Yang Z, Zheng J, Wei D. Artesunate induces ferroptosis in osteosarcoma through NCOA4-mediated ferritinophagy. *The FASEB Journal*. 2025;39:e70488. doi:10.1096/fj.202403160R